# An Evaluation of Optimal Friction Stir Welding Factors (FSWF) For Yellow Brass 405-20

**Syed Farhan Raza**
University of Engineering and Technology
**Sarmad Ali Khan**
University of Engineering and Technology
**Muhammad Salman Habib**
University of Engineering and Technology
**Naveed Ahmed**
Al Yamamah University
**Kashif Ishfaq**
University of Engineering and Technology
**Ahmed Mehdi** ( ahmed.mehdi@uqconnect.edu.au )
UQDI: The University of Queensland Diamantina Institute

**Research Article**

**Keywords:** Friction Stir Welding (FSW), Weld Temperature, Weld Hardness, Friction Stir Weld Strength (FSWS), Friction Stir Welding Factors (FSWF), Friction Stir Welding Zone (FSWZ)

**Posted Date:** January 11th, 2022

**DOI:** https://doi.org/10.21203/rs.3.rs-1226477/v1

# Abstract

Friction stir welding (FSW) is a green, environmentally amicable, and solid-state joining technology. FSW can successfully weld a wide range of materials (similar/dissimilar parent materials) including aluminum, copper, steel, different alloys from these materials, plastics, composites. FSW of brass has already been accomplished by fewer researchers. In this research, yellow brass 405-20 is, therefore, welded with FSW that was never welded before. In this study, tool material utilized was M2 HSS that was also novel. Effect of two friction stir weld factors (FSWF), rotational speed (RS) and traverse speed (TS), was found on three output parameters i.e., weld temperature, weld strength and weld hardness. Weld temperature developed, was found to be 63.72% of melting point of base metal. A significant improvement in friction stir weld strength (FSWS) was also measured that was found to be 106.37% of the base brass strength. Finally, weld hardness was measured which was found to be 87.80% of original brass hardness. Based on main effects, optimal FSW factors were found to be 1450 rpm and 60 mm/min resulting interestingly in optimal temperature, optimal weld strength, and optimal hardness. Rotational speed (RS) was found to be significant to affect the weld temperature only at the friction stir weld zone (FSWZ) with the highest percent contribution (PCR) of 65.69%. However, PCR of transverse speed was found to be maximum for affecting weld strength as compared to its PCR towards both weld temperature and weld hardness. Current study was also deepened by microscopic investigation.


# Introduction

Friction stir welding (FSW) is an innovative solid-state joining technique benefiting both industries and research laboratories because of its numerous returns e.g., it's fumeless, external medium-less or filler-less, melt-less due to its solid-state nature, no requirements of personal protective equipment, etc. FSW was first used for aluminum and its alloys at the Welding Institute of the United Kingdom and patented by Wayne Thomas in 1991 [1]. Now, it has become a state-of-the-art assembling technique that can be employed to weld a variety of materials other than aluminum e.g., steel, magnesium, copper, plastics, composites, and several combinations of dissimilar materials taking two dissimilar materials at a time of welding [2].

Brass is generally an alloy of copper and zinc. Brass properties mainly depend on heedful arrangements of percent copper in percent zinc. Brass has already become a good candidate for engineering and industrial applications owing to its striking properties such as high strength, high corrosion resistance, high electrical and thermal conductivities. Brass may easily be processed with exceptions to fusion welding processes, and it looks apparently nice before and after processing. However, brass provides a lot of difficulties when it's subjected to fusion welding which involves melting of brass, since fusing brass usually evaporates zinc leaving brass with porosity issues. Therefore, weldability studies on brass material are scarce. C. Meran et al. [3] reported welding problems associated with the brasses when they are fused by tungsten inert gas (TIG) pulse welding. Zinc evaporates at 907 $^{o}$C (boiling temperature of zinc) and porous appearance is achieved at the weld bead. The yellowish color of brass turns into reddish color due to the zinc evaporation. Although authors addressed severe difficulties in welding brasses, it

was an excellent effort of that time when it was hard too to find considerable studies on joining brass materials.

Hence a need arises for such a novel joining process which doesn't give rise to the melting of brass keeping it in its solid-state during and after welding to prevent zinc from evaporating. To fulfill this need, novel FSW may be used to join brass considering solid-state joining of brass. For instance, F. Hugger et al. [4] performed the laser beam welding of brass. They realized a huge evaporation of zinc, since fusion of brass happens during laser welding. Although the joining of brass via laser welding is novel, the joint properties of brass are expected to be greatly compromised due to the evaporation of zinc as weld interface temperature goes beyond 1200 $^{o}$C justifying the viability of FSW for brass. On the other hand, C. Meran [5] welded the brass (CW508L) using FSW. Author has validated that melting of brass was never observed leading to preserving excellent joint properties in the presence of zinc. Moreover, a welding efficiency of joint was achieved to be 94.44%.

G. Cam et al. [6] joined two brass alloys separately using FSW. Brass alloys used are 70/30 and 90/10. Authors have found microscopically that no porosity exists when joining these brass alloys with FSW. This validates that there is no evidence of evaporation of zinc during FSW of brass alloys. Therefore, it has been reconfirmed that FSW is a solid-state joining process. Although researchers have welded brass specimens with welding efficiency of 117% for 70/30 brass alloy and 98.88% for 90/10 brass alloy, other brass alloys could also be welded to explore further the FSW's potentials with excellent welding efficiencies. M. B. Durdanovic et al. [7] established a better comprehension of FSW by segregating it into five stages with a supposition that tool keeps rotating until all the FSW stages are covered. These phases are namely plunging the FSW tool into weld specimens, primary dwell, translation in a straight line, secondary dwell, and pulling the FSW tool out of welded specimens. In addition, authors have also settled a mathematical model to calculate the heat generation during FSW. Although authors have made an excellent effort to present comprehensive understanding of FSW, they did not take any welding material into account, this FSW understanding should be applied on novel materials like brass 405-20.

T. Murakami et al. [8] worked on the microstructural variations when joining brass using FSW. At friction stir weld zone (FSWZ), two phases recognized were named as alpha and beta phases. Alpha phase was the bright phase whereas the beta phase was dark phase. With a proper weld setting, beta phase was neglected owing to its presence up to 17 – 20% as compared to the base brass where degree of this phase was present to be 16%. Since evaporation of zinc was not observed even in a single welding situation, FSW was again verified as a solid-state joining technique. It was also found that alpha grain size reduces up to a certain degree with reducing the heat input. Maximum tensile strength of 398 MPa was reported by the authors, therefore, the welding efficiency was obtained to be 101% for 60/40 brass. This weld strength can also be reduced by mitigating defect's formation at the FSWZ owing to non-recrystallization of alpha phase of brass. A. Heidarzadeh et. al. [9] explored the microstructure of 63/37 brass to reveal the presence of any defects. They utilized optical microscope, scanning electron microscope (SEM), and scanning transmission electron microscope (STEM) to reveal the microstructure of brass under investigation. It was disclosed that the alpha grains turn into finer grains with FSW owing

to dynamic recrystallization (DR) after FSW. However, beta phase divides it between the alpha grains without DR. In this work, welding efficiency was acquired to be 88.85%.
Z. Y. Ma et al. [10] studied the effect of rotational speed on the FSW joint quality when joining brass. The welding efficiency was found to be 80% of parent material (PM). Although authors have achieved a good quality of joint, the specimen's dimensions were not following any ASTM standards and effect of transverse speed was also neglected. P. V. C. S. Rao et al. [11] tested the FSW joint of brass alloy using hardness test and many other tests. The hardness of joint was found to be higher than that of parent material. Although authors have conducted a good study on the FSW of brass, the hardness of joint should be lower than that of parent material to minimize the weld brittleness whose high value can be detrimental to joint quality.
Therefore, few studies were found on FSW of brass alloys. These studies may establish a strong foundation for trial experiments along with the results from numerical studies when novel brass materials/alloys are intended to be welded by FSW.

Few trial experiments are usually deemed to be essential with novel combinations of FSW factors in the light of relevant literature to determine the effect of FSW factors on response parameters. Sometimes, trial experiments seem essential in the absence of background knowledge as the most of the novel research studies are never conducted before. In this context, simulation studies can help researchers minimize the cost and time required for trial experiments. Therefore, validated numerical studies, based on thermo-mechanical settings, may be executed towards evaluating the suitability of weld factors which may lead to shrink the efforts required for trial experiments. The numerical studies have also economical advantage [12].

K. M. Rao et al. [13] performed a thermal simulation study for FSW of Al6061-T6 alloy. Ansys was used to perform the simulation studies. The numerical study was found to be in good agreement with the empirical study. The peak temperature at the FSWZ obtained was 69.2% of melting temperature of the material under investigation. Although authors provided the researchers with better understanding of heat calculations at the FSWZ, the peak temperature is approaching the melting point of Al6061-T6 and the samples' geometry was non-standard too. Z. Zhang et al. [14] also reported a full thermo-mechanical model to study the effect of shoulder size on the thermal distributions and material deformations in the FSWZ. In this work, the workpiece used was Al6061-T6 alloy. Authors found that temperature rise at the FSWZ directly depends on the shoulder size except the need for the boundaries of FSWZ where recrystallization is dominated by the material deformation. Since FSW is a solid-state joining technique, the maximum temperature rise noted at the FSWZ, was 63.8% of the melting temperature of workpiece material. Although authors provided the researchers with a better simulation methodology to address the temperature distributions at the FSWZ, the peak temperature is still reaching the melting point of Al6061-T6 and the samples were again non-standard too.

B. G. Kiral and H. T. Serindag [15] performed a numerical and experimental studies on FSW of Mg alloy (AZ31). Ansys APDL was used to conduct the numerical studies for temperature distributions. Hardness and joint strengths were also reported. The maximum temperature achieved was 450 $^{o}$C which was 75%

of the melting temperature of base material. Hardness achieved was 80% of the base material's hardness. Although authors have executed an excellent study on FSW numerically and empirically, the peak temperature is quite high and reaching the melting point of base material with hardness higher too. As higher hardness may result in increasing brittleness of joint.
M Song and R Kovacevic [16] presented the thermal studies on FSW addressing three dimensional (3D) transient thermal model using finite difference method. Numerical results were validated by the empirical FSW data with good agreement between these results. Although authors have delivered a unique numerical work, this thermal and numerical study should further be used for determining the joint strength. Moreover, authors used aluminum and tool steel in this study. Therefore, a research space for comprehensive study on brass material, still, exists which should be properly filled.

P. Biswas and N. R. Mandal [17] have established another thermal study finding mainly the tool geometry's effect on the thermal history using aluminum alloy. Numerical results were deduced to be agreed nicely with those of empirical confirming that the thermal study assumptions were appropriate. Although authors have delivered another good simulation idea, several vital aspects of FSW were not addressed e.g., standard weld sample design, effect of other possible FSW factors on thermal results, aluminum material replacement with other novel materials, etc.

H. Zhang et al. [18] executed a thermal study on magnesium alloy AZ31 that is a good candidate for FSW. This study is an effort towards investigation of thermal distribution for the preheating period of FSW looking for suitable preheating weld parameters. Although authors have finally studied numerically FSW of AZ31, similar kind of problems, still, exists including specimen design was not standardized and temperature measurement involves utilizing conventional k-type thermocouples.
S. Bag et al. [19] conducted a thermal analysis numerically and experimentally using aluminum alloys. In the study, heat input was given as a symmetric heat flux at the union line of flat tool shoulder surface, tool pin side, and bottom surfaces. Although numerical and empirical results were agreeing with each other, aluminum was considered again which should be replaced with any other novel material like brass. Moreover, effect of transverse tool speed was neglected. Similarly, A. R. S. Essa et al. [20] determined numerically the effect of eccentric cylindrical pin on the heat generation while FSW of aluminum alloy. Although the numerical study was again in good agreement with that of experimental, the same numerical and empirical studies may be applied to brass to validate whether a very good agreement, still, exists between numerical and empirical results or not.
H. A. Derazkola et al. [21] used a new numerical method using computational fluid dynamics (CFD) to understand how materials flow and mix together during FSW. They also worked on finding a link between the materials mixing and materials bonding before and after FSW respectively. Although this CFD approach was never used to understand the intermixing of materials during FSW of Al-Mg-Si alloy T-Joints, this numerical study was not validated with any empirical methods. Moreover, the material flow during FSW like a fluid is unlikely, since materials to be welded remain in solid-state during FSW.
From the literature on FSW, it is obvious that limited researchers have welded brass as welding problems may arise from fusion welding of brass. Researchers have welded various materials other than brass employing FSW process factors. In fact, researchers have tried their best to improve the welding efficiency

in term of various output parameters/responses which include joint strength, joint hardness, and joint temperature. A study gap inevitably exists to improve these output parameters for brass material. Statistical analysis is also found to be scarce on the way to FSW of brass. Therefore, a thorough statistical analysis involving main effects, interaction plots, PCRs of each friction stir welding factor (FSWF), was a need of the time. Numerical and empirical studies on FSW of brass were also limited too; with good agreement in them. Although H13 HSS is frequently used for FSW, effect of new tool material e.g. M2 tool steel was never investigated. As far as research methods are concerned, many researchers used k-type thermocouples to measure weld temperature which are economically full of wastage in terms of time, cost, precision, and accuracy. Hence precise temperature measuring devices might be used which could save time and money. In this study, a noncontact thermal camera was used instead of contact thermocouples. In fact, improvements of weld strength, weld hardness, and weld temperatures pertinent to friction stir welding of brass 405-20, were never studied before and their interrelationships. Present study is an effort to cover these research gaps highlighted towards FSW of brass 405-20.

## Materials And Methods

Materials and methods section for Friction stir welding (FSW) process can be divided in to two categories to make it more eloquent. One is named as the pre-welding and second is termed as post-welding.

# 1.1. Pre-Welding

In this category of materials and methods, description of research settings, will be discussed which was accomplished before welding. Customized FSW was established using computer numerically controlled (CNC) machining centre to weld brass 405-20. A general FSW process is shown in Fig. 1 and customized FSW set up with CNC is shown in Fig. 2. An adjustable CNC program was written with considerations to spindle speed function (S) to account for rotational speed of FSW tool and feed function (F) to specify the traverse speed of FSW tool. Penetration depth of FSW tool pin was also specified in the program in terms of its value in z-axis. Likewise, nine experiments were performed with planned alterations to the values of S & F in CNC program as per the design of experiments (DOE) which is based on full factorial method and factors' levels, as shown in Tables 2 and 1 respectively. Moreover, revolutionary pitch is the ratio of rotational speed and traverse speed of the FSW tool, as shown in Table 2. Important brass 405-20 properties are shown in Table 3, 4, & 5. Specimens were fabricated as per guidelines of the ASTM standard (E8/E8M-13a), as shown in Fig. 3.

Table 1
Factors' Levels for FSW of Brass

| Weld Factors | Level 1 | Level 2 | Level 3 |
|---|---|---|---|
| Rotational/Spindle Speed (rpm) | 1600 | 1450 | 1300 |
| Traverse/Welding Speed (mm/min) | 60 | 50 | 40 |

Table 2
L-9 DOE based on Full Factorial Method

| Sr. No | Rotational Speed (Revolution per min) | Traverse Speed (mm/min) | Revolutionary Pitch (Revolution per mm) |
|---|---|---|---|
| 1 | 1600 | 60 | 26.67 |
| 2 | 1600 | 50 | 32.00 |
| 3 | 1600 | 40 | 40.00 |
| 4 | 1450 | 60 | 24.17 |
| 5 | 1450 | 50 | 29.00 |
| 6 | 1450 | 40 | 36.25 |
| 7 | 1300 | 60 | 21.67 |
| 8 | 1300 | 50 | 26.00 |
| 9 | 1300 | 40 | 32.50 |

Table 3
Chemical Composition of Brass

| Material | Cu | Zn | Pb | Sn |
|---|---|---|---|---|
| | Percentage (%) | | | |
| Brass 405-20 | 63.0 | 34.7 | 1.0 | 1.0 |

Table 4
Mechanical Properties of Brass

| Material | UTS (MPa) | Yield Strength (MPa) | Hardness (HR-15N) | Elongation (%) |
|---|---|---|---|---|
| Brass 405-20 | 275 | 250 | 82 avg. | 15 |

Table 5
Thermal Properties of Brass

| Material | Specific Heat (C) | Thermal Conductivity (K) | Density (ρ) | Emissivity (ε) | Melting Point (Tm) |
|---|---|---|---|---|---|
| | J/kg $^{o}$C | W/m $^{o}$C | Kg/m3 | (600$^{o}$C) | $^{o}$C |
| Brass 405-20 | 380 | 119 | 8800 | 0.61 | 940 |

Yellow brass 405-20 is an alloy of coper 63%, Zinc 34.7%, and little traces in percentage of lead and tin. This alloy has good corrosion properties. Specimens were manufactured in two halves, as shown in Fig. 4. Wire electric discharge machining (EDM) was used to fabricate the samples. Filing process and emery tapes were used to prepare surfaces of the fabricated samples prior to welding.

Molybdenum high speed tool steel (M2 HSS) was chosen and utilized as a tool material. M2 HSS is chemically composed of 5 to 9.5 percent of molybdenum, nearly 4 percent chromium, 1.5 to 6.5 percent tungsten, and smaller traces of vanadium. M2 HSS has approximately similar properties to those of the H20 to H26 steels with an economic merit of minor initial cost. M2 HSS has also the increased resistance to thermal fatigue which implies greater resistance to high temperature softening over a longer period.

M2 HSS was procured in the form of cylindrical rods. M2 HSS rods were turned employing a conventional lathe machine with required operations which comprise cutting off, facing, and turning to obtain finally the diameters of shoulder and pin, as shown in Fig. 5.

A fixture was also designed and manufactured on conventional machining center to hold the specimens so that specimens will not be allowed to move in x, y, and z directions, as shown in Fig. 6. Supporting strips were also used to fix the open sides of FSWZ of specimens for effective welding without permitting any lateral movement during FSW. Moreover, FSW tool enters the supporting strip on one side, transverses while rotating along the weld line of specimens, and leaves the specimens from the other supporting side, as can be seen in Fig. 7.

Moreover, a thermal imager having model number 868, supplied by Testo, was also used at the time of welding brass specimens to measure the temperature distributions at FSWZ, as shown in Fig. 8. Thermal imager does not only measure the maximum temperature during FSW but it also reveals the numerous values of temperatures i.e., temperature distributions can easily be measured at any location of FSWZ that is just a one mouse click away. In the past, researchers have used k-type of thermocouples for measuring the temperature strictly for only one location of weld zone which is not only time-consuming but also thermocouples' usage does not provide an opportunity to measure the joint strength and hardness later due to the presence of thermocouple wires at FSWZ after welding. Thermal imager appears to be competent in fixing the time and effort issues during and after welding. Moreover, testo IRSoft software version 4.7 is essentially installed and utilized for processing of thermal images resulting in measurements of the multiple zonal temperatures, as shown in Fig. 9 for DOE 4. In processing a thermal image, four interfaces are usually obtained comprising top left interface that shows the likely multiple locations of hot spot (HS) and cold spot (CS) which are the maximum and minimum temperature respectively during FSW, top right interface represents the temperature scale or maximum and minimum values of temperature scale illustrating the temperature color scheme, bottom left interface shows the values of CS and HS, and bottom right interface depicts the actual welding scenario picture similar to a snapshot that may be taken from ordinary photo camera. Various HS and CS points can be measured and recorded simply by clicking mouse buttons at different locations of top left interface. The recorded HS is the peak likely value of HS at FSWZ obtained from FSW of brass.

# 1.2. Post-Welding

In this section of materials and methods, a detailed account of experimental investigation is elaborated that was accomplished after welding brass.

Maximum temperatures have already been registered with the usage of thermal camera at the real time of FSW of brass. Supporting side strips welded with the specimens were removed using an electric saw, as can be seen in Fig. 10. Having cut via electric saw, the weld specimen according to definitions of ASTM standard, is now ready for further tests, as shown in Fig. 11. Welded specimens were tested for their joint strength and hardness. Furthermore, friction stir weld strength (FSWS) was tested using a tensometer with a crosshead speed of 1mm/min, as shown in Fig. 12. Three samples were tested for each welding experiment resulting in average of weld strengths and weld temperatures. A broken tested specimen is also depicted in Fig. 13. For measuring hardness, Rockwell hardness testing machine was used considering various points of the joint, as shown in the Fig. 14. Mean of hardness values was also then calculated. And hardness value is also the average of two values of hardnesses at the FSWZ, as shown previously in Fig. 7.

## Results And Discussion

Results are analyzed statistically using analysis of variance (Anova), percent contributions (PCRs), and interaction plots (IPs). It is a considered view that Anova is a powerful indicator of weld factor's significance or insignificance. Anova was performed at 95% confidence level implying that any weld factor will be considered significant if it's p-value were less than 0.05 and vice versa. On the other hand, PCRs and IPs are associated with both significant as well as insignificant weld factors. PCR indicates the contribution of each factor in percentage towards the output response without considering their significance. IPs determine whether there exists any combined effect of two or more factors on the output response which can result in increasing the error PCR. Therefore, friction stir welding factors (FSWF) may be evaluated for their definite and detailed effects on the weld quality/output responses with the help of Anova, PCRs, and IPs.

Conclusively, effect of FSWF (mainly rotational speed (RS) and traverse speed (TS)) on the three output responses is being presented and discussed in the light of Anova, PCRs and IPs.

# 2.1. Effect of FSWF on Weld Temperature

Anova indicates that rotational speed is the only FSWF which was found to be significant towards affecting weld temperature at FSWZ, as can be seen from Anova Table 6. Although the p-value for the traverse speed is closer to 0.05, it is insignificant towards affecting the weld temperature. Therefore, it will be interesting to determine the PCR of traverse speed i.e., 24.77%, as can be seen in the last column of Table 6. Hence traverse speed is insignificant at 95% confidence level, however, this weld factor is necessary to be there as it is contributing by 24.77% to develop a good weld temperature. A better weld temperature rather good implies that it should not exceed the melting temperature of brass 405-20 which is the spirit of FSW as a solid-state joining technique. Similarly, PCR of rotational speed is 65.69% with its significance towards affecting the weld temperature. Finally, IP will be seen to again examine any chance of combined effect of rotational speed and traverse speed to comment further on both insignificance of traverse speed and PCR of error. Since the error PCR is extremely small i.e., 9.54%, there is a strong

possibility of minimal interaction or independence between RS and TS, as shown in Fig. 15. Additionally, the optimal levels of FSWF for maximum weld temperature, are 1450 rpm and 60 mm/min, as shown in main effects' Fig. 16. Another plot showing the weld temperature pattern for the complete 9 DOEs, is shown in Fig. 17.

Table 6
Anova Table for Weld Temperature

| Source | DF | Seq SS | Adj SS | Adj MS | F | P | PCR |
|---|---|---|---|---|---|---|---|
| Rotational Speed (RPM) | 2 | 12293.40 | 12293.40 | 6146.70 | 13.78 | 0.02 | 65.69 |
| Traverse Speed (mm/min) | 2 | 4635.10 | 4635.10 | 2317.50 | 5.19 | 0.08 | 24.77 |
| Error | 4 | 1784.80 | 1784.80 | 446.20 | | | 9.54 |
| Total | 8 | 18713.30 | | | | | |

# 2.2. Effect of FSWF on Weld Strength

As far as the effect of rotational speed and traverse speed on weld strength is concerned, none of these two FSWF were significant, as can be seen under the P column of Table 7. So, there is enough need to examine the PCRs and the presence of any interaction between these two FSWF. Firstly, the last column of Table 7 shows the PCRs for rotational speed, traverse speed, and error. The PCR of traverse speed is almost four times the PCR of rotational speed implying that the contribution in percentage of traverse speed is significantly higher towards acquiring a better weld bead. On the other hand, error PCR is little bit higher i.e., 27.20% justifying sufficiently the reason for having a closer look at the presence of any interaction between rotational speed and traverse speed. Interaction plot between these two FSWF is shown in Fig. 18. There is a complete absence of any interaction between the levels of traverse speed for 1300 rpm and 1600 rpm. There exist two interactions of uniform severity indices (SI) of 38.90% between 1450&1300 rpm and 1450&1600 both at a region of traverse speed of 40 to 50 mm/min. Therefore, a combined effect of 1300 and 1600 with 1450, has now been identified at two levels of traverse speed 40&50 mm/min. This combined effect of identified levels of both FSWF is the main reason for higher error PCR. Interestingly, the optimal levels of FSWF for optimal weld strength, are again found to be 1450 rpm and 60 mm/min, as illustrated in main effects' Fig. 19. This validates that 1450 rpm and 60 mm/min are those levels of rotational speed and traverse speed which deliver both optimal weld temperature and optimal weld strength. Moreover, optimal weld temperature is evidently the cause of optimal weld strength as a result. Finally, the graph of weld strengths for each DOE is shown in Fig. 20.

Table 7
Anova Table for Weld Strength

| Source | DF | Seq SS | Adj SS | Adj MS | F | P | PCR |
|---|---|---|---|---|---|---|---|
| Rotational Speed (RPM) | 2 | 854.00 | 854.00 | 427.00 | 1.10 | 0.42 | 14.97 |
| Traverse Speed (mm/min) | 2 | 3298.70 | 3298.70 | 1649.30 | 4.25 | 0.10 | 57.83 |
| Error | 4 | 1551.30 | 1551.30 | 387.80 | | | 27.20 |
| Total | 8 | 5704.00 | | | | | |

# 2.3. Effect of FSWF on Weld Hardness

Effect of FSWF is also insignificant towards affecting the weld hardness, as shown in Table 8. PCR of RS is found to be 42.18% which is ten times more than that for TS i.e., 4.08%. However, the error PCR is considerable which is 53.74% implying that there exists greater possibility for interdependence of various levels of both RS and TS. This interdependence or combined effect of FSWF's levels may be clearly examined by looking at the interaction pots, as shown in Fig. 21. Of the interaction plot, it can be easily realized that two interactions are severe in the TS range from 40 to 50 mm/min. First interaction is between 1300 & 1600 rpm having a severity index (SI) of 98.90% and second is between 1300 & 1450 rpm with SI of 83.33%. In the 50 to 60 mm/min region of TS, a third interaction of RS is also present that is between 1300 & 1600 rpm having a SI of 65.56%. Though the effects of FSWF on weld hardness are insignificant and error PCR is high too, severe interaction plots eloquently reveal the reasons of insignificant FSWF and high error PCR in term of combined effects of RS and TS on weld hardness. Hence influence of interdependency of RS and TS (both independent FSWF) is dominantly higher based on the SI as compared to those for weld strength as FSWF do not have any interaction for affecting the weld temperature. Of the main effects' plot shown in Fig. 22, weld hardness is the lowest at the same FSWF which were identified to be optimal FSWF for weld temperature and weld strength i.e., 1450 rpm and 60 mm/min. Weld hardness is desired to be lower after welding as higher weld hardness may increase the brittleness of the FSWZ due to the presence of various intermetallic compounds. Finally, a graph between the weld hardness and DOEs is presented in Fig. 23.

Table 8
Anova Table for Weld Hardness

| Source | DF | Seq SS | Adj SS | Adj MS | F | P | PCR |
|---|---|---|---|---|---|---|---|
| Rotational Speed (RPM) | 2 | 82.67 | 82.67 | 41.33 | 1.57 | 0.31 | 42.18 |
| Traverse Speed (mm/min) | 2 | 8.00 | 8.00 | 4.00 | 0.15 | 0.86 | 4.08 |
| Error | 4 | 105.33 | 105.33 | 26.33 | | | 53.74 |
| Total | 8 | 196.00 | | | | | |

Interestingly, the optimal FSWF are found to be 1450 rpm and 60 mm/min for all the three output or dependent variables. This again validates in one way the effectiveness of the results in the current

research settings that optimal FSWF are deduced to be similar and linked with their physical explanations as well, for weld temperature, weld strength, and weld hardness. This is now obvious that optimal weld temperature definitely gives rise to optimal weld strength which both are desired to be the maximum. However, these two optimal FSWF can only result in optimal responses if lower weld hardness were quantified at the FSWZ.

## 2.4. Validation Experiments for Optimal FSWF

Three validation experiments were conducted after getting optimal FSWF identified for weld temperature, weld strength, and weld hardness. Moreover, weld temperature is further validated via thermal simulation based on FEA. Weld hardness is measured again in the same fashions, as described in the materials and methods section. Furthermore, three samples were tested with optimal FSWF settings to validate the weld temperature, weld strength, and weld hardness.

### 2.4.1. Validation of Weld Temperature

After setting the optimal FSWF on the customized CNC FSW, three validation experiments were performed for three samples and weld temperature for its maximum value was measured using thermal imager, as shown in Table 9. The average value of weld temperature was found to little higher than the maximum value obtained from nine experiments of DOE i.e., 599 $^{o}$C. This value of peak weld temperature is 63.72% of the melting temperature of brass 405-20. Hence weld temperature remained below the melting temperature of the parent material again validating the solid-state joining spirit of FSW. Upon focusing on the literature, brass was rarely joined by FSW. For instance, F. Hugger et al. [4] joined the brass with laser beam welding process. The weld temperature went up to 1200 $^{o}$C which was beyond the melting point of brass resulting in evaporation of Zn leaving the weld interface with porosity issues. This was the only one thermal study found towards joining brass. However, many researchers have joined aluminum using FSW. For instance, K. M. Rao et al. [13] performed a thermal simulation study for FSW of Al6061-T6 alloy. The percent of melting temperature was 69.2% was obtained as a peak temperature at the FSWZ. Although the peak weld temperature is lower than that of the parent aluminum material, the weld temperature is found to be higher than that of weld temperature of current study on brass i.e., 63.72% which should be lower to avoid the alloying materials from evaporating and degrading. Z. Zhang et al. [14] also reported the weld temperature for FSW of Al6061-T6. The maximum temperature rise was noted to be 63.80% of the melting temperature of workpiece material at the FSWZ that is again higher than what was achieved in this study. B. G. Kiral and H. T. Serindag [15] performed a numerical and experimental studies on FSW of Mg alloy (AZ31). The peak weld temperature achieved was 450 $^{o}$C which was 75% of the melting temperature of base material leading to welcome various welding issues as weld temperature is reaching the melting point of parent material. Therefore, peak weld temperature of current study obtained was found to be the better than any FSW study on brass and even for other materials e.g., aluminum and magnesium. Moreover, a thermal simulation was also performed known as transient thermal analysis, as shown in Fig. 24, to validate the optimal weld temperature and a good agreement was found in the empirical and numerical values, as shown in Fig. 25, of optimal weld temperature with little error. A little description of thermal study is presented here.

Table 9
Validation Experiment for Weld Temperature

| Sr. No | Rotational Speed (Revolution per min) | Traverse Speed (mm/min) | Weld Temperature ($^oC$) | Average Weld Temperature ($^oC$) |
|---|---|---|---|---|
| 1 | 1450 | 60 | 595 | 599.67 |
| 2 | 1450 | 60 | 599 | |
| 3 | 1450 | 60 | 605 | |

Eq. 1 [23] is the governing differential equation for calculating weld temperature numerically.

$k\,\partial^2T/\partial x^2 + k\,\partial^2T/\partial y^2 + k\,\partial^2T/\partial z^2 + Q - \rho c\partial T/\partial t = 0$ (1)

Where,

T = Temperature, $^oC$ (to be determined by solving Eq. 1)

K = Isotropic Thermal Conductivity, W/m. $^oC$

ρ = Density, $Kg/m^3$

c = Specific Heat Capacity, J/Kg. $^oC$

Q = Volumetric Heat Generation Rate, W/m3. $^oC$

Meshing of the geometry was achieved once the geometrical model was assigned with brass material properties mentioned in Table 3, 4 & 5. Moreover, mesh verification was accomplished with three levels of meshing which are; low, medium, and high quality. Maximum weld temperature found for these three qualities of meshing was almost similar. Hence mesh medium quality was selected for the thermal simulation.

Volumetric heat generation rate (Q) was given as an input heat flux at the joint interface in thermal simulation to foresee the peak weld temperature at FSWZ. Average power generation (q) during friction stir welding was calculated by Eq. 2 and heat flux per unit area (Q) was calculated by Eq. 4 [24].

$$q = 2\pi * k * \omega * Rs^3/3$$

2
Where,

k = yield stress of brass (MPa)

ω = Rotational Speed (rad/s)

$R_S$ = Shoulder Radius

$$Q = \frac{3 * q * Rs}{Rs^3 - Rp^3} (3)$$

Where,

q = Eq. 2

$R_P$ = Pin Radius

Moreover, when putting q in Eq. 3, a mathematical relationship is obtained for heat flux per unit area that is shown in Eq. 4.

$$Q = \frac{k * \omega * Rs^4}{Rs^3 - Rp^3} (4)$$

Since Eq. 4 considers only the heat flux owing to conduction at the weld interface, heat losses due to convection from the FSWZ into the environment or air, have also been calculated using fundamental equation of convection heat transfer, as shown in Eq. 5.

$Q_{convection} = h * (Ts - Ta)$ (5)

Where,

h = film coefficient

Ts = Surface Temperature at the weld interface

Ta = Air/Ambient Temperature

Moreover, the surface temperature at the weld interface, was measured using transient thermal analysis. And film coefficient (h) was calculated then by putting Q from Eq. 4 equal to $Q_{convection}$ from Eq. 5.

# 2.4.2. Validation of Weld Strength

Friction stir weld strength (FSWS) was also validated by conducting three experiments with optimal FSWF's levels setting, as shown in Table 10. Average value of FSWS was achieved to be 227.67 MPa implying weld efficiency to be 106.37% showing an improvement in weld quality towards the limited efforts of joining brass in the literature. For instance, Z. Y. Ma et al. [10] found the welding efficiency to be 80% of parent brass which is lower than that from current study. Although there were present few studies on FSW of different grades of brass having welding efficiency greater than that for the current study, present work is an effort of joining a unique grade of brass finding its considerable place in the literature. For example, A. Heidarzadeh et. al. [9] found the FSWS of 63/37 brass. They have found the welding efficiency to be 88.85%. C. Meran [5] found the welding efficiency of joint to be 94.44% for brass

(CW508L). G. Cam et al. [6] joined two brass alloys using FSW separately. Brass alloys used are 70/30 and 90/10. They found the welding efficiency of 98.88% for 90/10 brass alloy and 117% for 70/30 brass alloy. T. Murakami et al. [8] have obtained the welding efficiency to be 101% for 60/40 brass. Therefore, the current study has found its place in the literature because of its higher value than those for other past studies.

Table 10
Validation Experiment for Weld Strength

| Sr. No | Rotational Speed | Traverse Speed | Weld Strength | Average Weld Strength |
|---|---|---|---|---|
| | **(Revolution per min)** | **(mm/min)** | **(MPa)** | **(MPa)** |
| 1 | 1450 | 60 | 292.14 | 292.54 |
| 2 | 1450 | 60 | 293.91 | |
| 3 | 1450 | 60 | 291.57 | |

## 2.4.3. Validation of Weld Hardness

Likewise, weld hardness was also validated by setting the optimal FSWF for three experiments, as shown in Table 11. The average weld hardness was acquired to be 72.00 that is 87.80% of the parent brass hardness. Extremely limited research efforts have been made to quantify the weld hardness in literature. Only one study has been found on FSW of brass for quantifying the weld hardness such as B. G. Kiral and H. T. Serindag [15] who found the weld hardness to be 80% of the base material's hardness which is lower than that was found in current study. Hence weld hardness is approaching the parent material hardness also showing the improvement in the joint quality. In this work, weld hardness is not more than that of the parent brass material. Weld hardness that is higher than that of the parent material hardness, may give rise to brittleness at the joint interface degrading the weld quality.

Table 11
Validation Experiment for Weld Hardness

| Sr. No | Rotational Speed | Traverse Speed | Weld Hardness | Average Weld Hardness |
|---|---|---|---|---|
| | **(Revolution per min)** | **(mm/min)** | **(HR-15N)** | **(HR-15N)** |
| 1 | 1450 | 60 | 72 | 72.00 |
| 2 | 1450 | 60 | 71 | |
| 3 | 1450 | 60 | 73 | |

## Microscopic Investigation

Fractography of fractured samples and microscopy of welded specimens were conducted after the samples have been welded and tested under tensile loading. Coordinate measuring machine(CMM) was used to perform the microscopy and fractography. Three magnification levels were used where appropriate including 70x, 30x, and 10x. 70x implies enhancing the magnification of any geometrical

feature up to 70 times and so on with 30x and 10x. A collection of amazing features has been revealed on the way to thorough microscopic examinations. For instance, interesting and beautiful circular patterns were seen at the pin entrance and ripples on the brass welded surface, as shown in Fig. 26. These two microscopic features were present in almost all the welded samples.

Of the Fig. 27, a small portion of uniform friction stir weld line can be seen within the actual size weld line which is also an essential result of friction stir welding of brass. Moreover, an irregular thin brass material was also found surrounding the weld line that is different from the parent brass and welded brass, as shown in Fig. 27

Fractured edges and surfaces are also shown in the Fig. 28 that are found nearly alike in all the welding experiments. As can be seen from Fig. 29, the cracks were also found within the welding zone which not only a probable cause of reducing weld strength but also pointing towards those welding experiments which may result in low weld strength. In this regard, the need for optimizing the weld strength was confirmed to find out those optimal weld factors or optimal welding experiments which would result in optimal weld strength.

# Conclusions

In this work, brass 405-20 was friction stir welded using two weld factors namely rotational speed and traverse speed. Full factorial design of experiments (DOEs) was implemented for both in this research work. Three response parameters were focused mainly including thermal distribution at FSWZ, joint strength, and hardness at the FSWZ. Anova, PCRs and interaction plots have been carefully examined to find and interpret the meaningful results.

Following were the main findings with current FSW research settings as explained earlier:

- All the FSWF were found to be insignificant towards affecting weld temperature, weld strength, and weld hardness except rotational speed as significant FSWF to affect weld temperature.
- Optimal FSW factors' levels were found to be 1450 rpm and 60 mm/min for DOE4 in full factorial settings to affect three output responses when finding them from main effects plots.
- Error PCR was negligibly found to be 9.54% for Anova of weld temperature indicating there is not interaction or combined effect of RS and TS on weld temperature. In other words, effect of both RS and TS is independent of each other towards affecting weld temperature.
- Error PCR of 27.20% was achieved for Anova of weld strength indicating there is possibility of getting FSWF's effects combined. Equal SI of 38.90% for both FSWF were found from the interaction plot for weld strength.
- Error PCR was found to be 53.74% for Anova of weld hardness. Therefore, the SI of more than 98% was found for FSWF. Hence combined effects of FSWF are dominating the independent effects of FSWF to affect the weld hardness.

- Maximum temperature was found to be 599 $^{O}$C which was well below the melting point of brass. So, successful friction stir welding of brass was validated in terms of its basic definition of solid-state welding. This temperature was also found for DOE4.
- Maximum joint strength was found to be 227.67 MPa at DOE4 which is 106.37% of base brass. Microscopy of joint surfaces can really help us present the causes of reduction in welding strength.
- Hardness was found to be the lowest for DOE4 and lower than that of the parent brass i.e., 72 HR validating further that DOE4 is an optimal combination of both rotational speed and traverse speed.
- Therefore, DOE4 can also be declared as the most optimal experiment among DOEs towards achieving excellent friction stir welding characteristics in terms of weld temperature, weld strength, and weld hardness.

# Declarations


### Acknowledgements

This work is based on the research initiatives for friction stir welding of brass by the first author i.e. Syed Farhan Raza. Moreover, the authors are really indebted to the University of Engineering and Technology, Lahore, Pakistan for the research facilities used in this research.


### Authors' contribution

Syed Farhan Raza: Conceptualization, Data analysis, Resources, Methodology, Writing-original draft, Sarmad Ali Khan: Methodology, Data analysis, Writing, Investigation, Muhammad Salman Habib : Methodology, Data analysis, Writing, Investigation, Naveed Ahmed: Review & editing, Kashif Ishfaq: Resources, Review and editing, Data analysis and curation, Ahmed M. Mehdi: Data curation, Review & editing.


### Funding

The current research work does not have any funding to accomplish current research.


### Data availability

The data related to experimental findings is already reported within the paper, and it can also be available from corresponding author 'Ahmed M. Mehdi' upon a reasonable request.

### Competing interests

The authors state that they have no conflict of interest or personal relationships that could have appeared to influence this work.

### Ethics approval and consent to participate

The authors confirm that they have abided by the publication ethics, state that this work is original, and have not been used for publication anywhere before.

### Consent for publication

The authors give consent to the journal regarding the publication of this work.

# References


1. He X, Gu F, Ball A (2014) A review of numerical analysis of friction stir welding., ” Prog Mater Sci 65:1–66. doi: 10.1016/j.pmatsci.2014.03.003
2. Overview J, Laska A (2020) “Properties of Butt Friction Stir Welded,” pp.1–46,
3. Meran C, Yuksel M, Gulsoz A, Sekercioglu T (2004) Welding problems with thin brass plates and tungsten inert gas pulse welding., ” Sci Technol Weld Join 9(2):131–137. doi: 10.1179/136217104225017053
4. Hugger F, Hofmann K, Stein S, Schmidt M (2014) Laser beam welding of brass., ” Phys Procedia 56:576–581. doi: 10.1016/j.phpro.2014.08.045
5. Meran C (2006) The joint properties of brass plates by friction stir welding., ” Mater Des 27(9):719–726. doi: 10.1016/j.matdes.2005.05.006
6. Çam G, Serindağ HT, Çakan A, Mistikoglu S, Yavuz H (2008) The effect of weld parameters on friction stir welding of brass plates., ” Materwiss Werksttech 39(6):394–399. doi: 10.1002/mawe.200800314
7. Durdanović MB, Mijajlović MM, Milčić DS, Stamenković DS (2009) Heat generation during friction stir welding process., ” Tribol Ind 31(1–2):8–14
8. Park HS, Kimura T, Murakami T, Nagano Y, Nakata K, Ushio M (2004) Microstructures and mechanical properties of friction stir welds of 60% Cu-40% Zn copper alloy., ” Mater Sci Eng A 371:1–2., pp. 160–169, doi: 10.1016/j.msea.2003.11.030
9. Heidarzadeh A, Barenji RV, Khalili V, Güleryüz G (2018) “Optimizing the friction stir welding of the α/β brass plates to obtain the highest strength and elongation,” *Vacuum*, vol. 159, no. August pp. 152–160, 2019, doi: 10.1016/j.vacuum.2018.10.036
10. Xie GM, Ma ZY, Geng L (2008) Effects of friction stir welding parameters on microstructures and mechanical properties of brass joints., ” Mater Trans 49(7):1698–1701. doi: 10.2320/matertrans.MRP2008089
11. Chandra Sekhara Rao PV, Ramesh Chandra B, Manoj A (2020) “The study of surface integrity on friction stir welded brass plates,” *AIP Conf. Proc.*, vol. 2269, no. October, doi: 10.1063/5.0019656
12. Neto DM, Neto P (2013) Numerical modeling of friction stir welding process: A literature review., ” Int J Adv Manuf Technol 65:1–4., pp. 115–126, doi: 10.1007/s00170-012-4154-8
13. Prasanna P, Subba Rao B, Krishna Mohana Rao G (2010) Experimental and numerical evaluation of friction stir welds of AA6061-T6 Aluminium alloy., ” J Eng Appl Sci 5(6):1–18

14. Zhang Z, Liu YL, Chen JT (2009) Effect of shoulder size on the temperature rise and the material deformation in friction stir welding., ” Int J Adv Manuf Technol 45:9–10., pp. 889–895, doi: 10.1007/s00170-009-2034-7
15. Serindag HT, Kiral BG (2017) Friction stir welding of AZ31 magnesium alloys – A numerical and experimental study., ” Lat Am J Solids Struct 14(1):113–130. doi: 10.1590/1679-78253162
16. Song M, Kovacevic R (2004) “Heat transfer modelling for both workpiece and tool in the friction stir welding process: A coupled model,” *Proc. Inst. Mech. Eng. Part B J. Eng. Manuf.*, vol. 218, no. 1, pp. 17–33, doi: 10.1243/095440504772830174
17. Biswas P, Mandal NR (2011) “Effect of tool geometries on thermal history of FSW of AA1100,” *Weld. J.*, vol. 90, no. 7,
18. Zhang H, Huang JH, Lin SB, Wu L, Zhang JG (2006) “Temperature simulation of the preheating period in friction stir welding based on the finite element method,” *Proc. Inst. Mech. Eng. Part B J. Eng. Manuf.*, vol. 220, no. 7, pp. 1097–1106, doi: 10.1243/09544054JEM425
19. Yaduwanshi DK, Bag S, Pal S (2015) “Heat transfer analyses in friction stir welding of aluminium alloy,” *Proc. Inst. Mech. Eng. Part B J. Eng. Manuf.*, vol. 229, no. 10, pp. 1722–1733, doi: 10.1177/0954405414539297
20. Essa ARS, Ahmed MMZ, Mohamed AKYA, El-Nikhaily AE (2016) An analytical model of heat generation for eccentric cylindrical pin in friction stir welding., ” J Mater Res Technol 5(3):234–240. doi: 10.1016/j.jmrt.2015.11.009
21. Memon S, Murillo-Marrodán A, Lankarani HM, Aghajani Derazkola H (2021) Analysis of friction stir welding tool offset on the bonding and properties of al–mg–si alloy t-joints., ” Materials (Basel) 14(13):1–18. doi: 10.3390/ma14133604
22. Patel V, Li W, Wang G, Wang F, Vairis A, Niu P (2019) Friction stir welding of dissimilar aluminum alloy combinations: State-of-the-art., ” Metals (Basel) 9(3). doi: 10.3390/met9030270
23. Suresh KS, Rani MR, Prakasan K, Rudramoorthy R (2007), doi: Modeling of temperature distribution in ultrasonic welding of thermoplastics for various joint designs., ” vol. 186:, pp. 138–146. 10.1016/j.jmatprotec.2006.12.028
24. Colegrove PA (2007) “Process Modelling, Chapter 10 in Friction Stir Welding and Processing. ” in Friction Stir Welding and Processing. ASM International, pp 187–217

# Figures

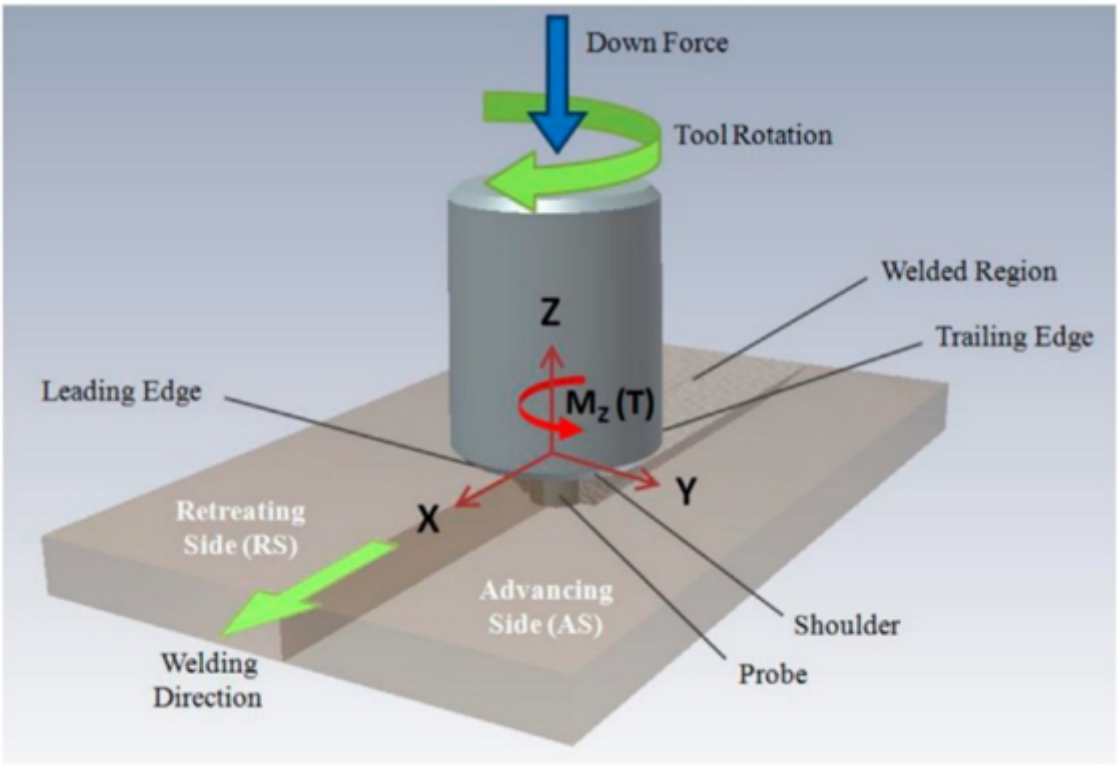


**Figure 1**

Friction Stir Welding [22]

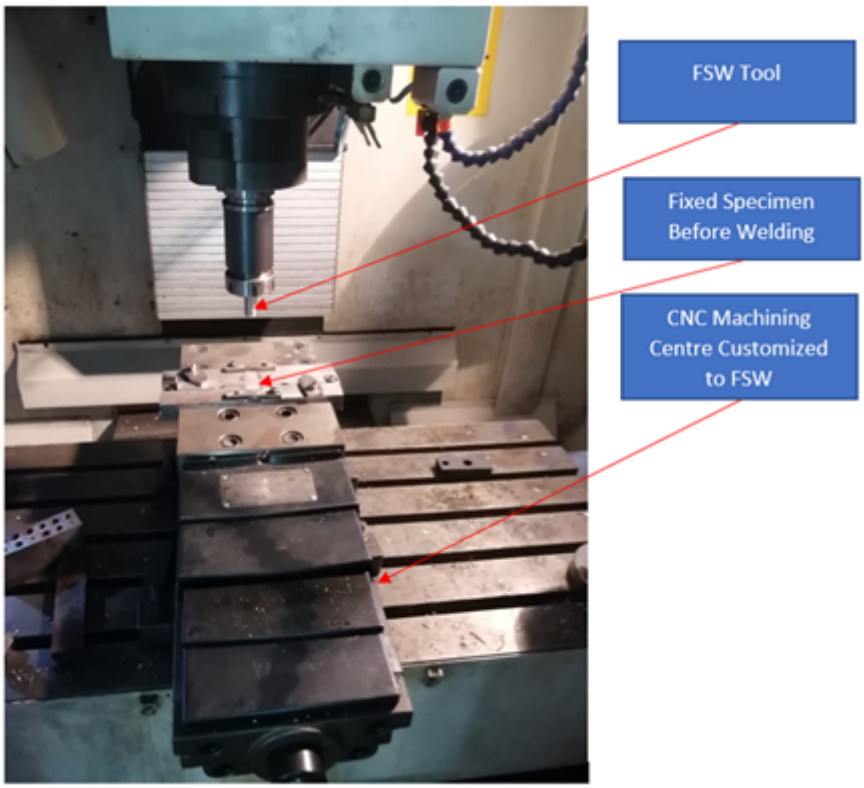

**Figure 2**

Customized FSW using CNC Machining Centre

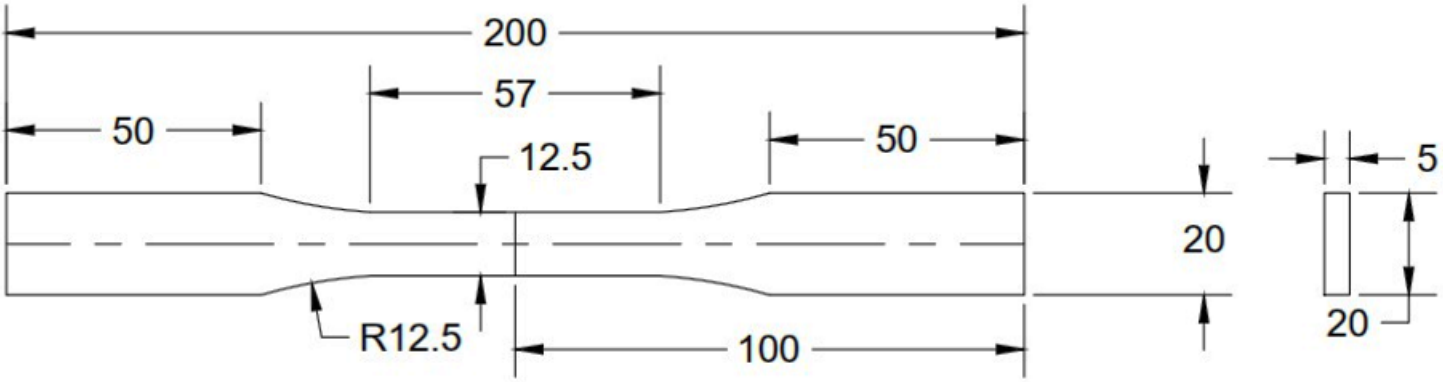


**Figure 3**

ASTM Standard (E8/E8M-13a) for Weld Specimen Design

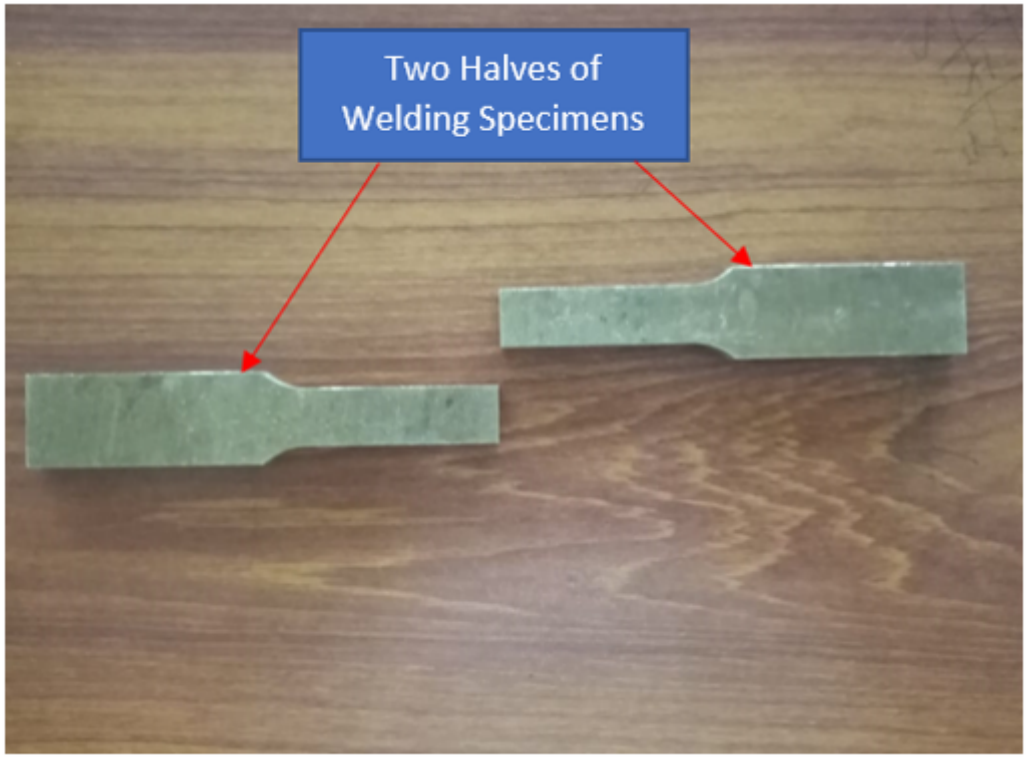


**Figure 4**

Manufactured Specimens as per ASTM Standard E8/E8M-13a in two halves

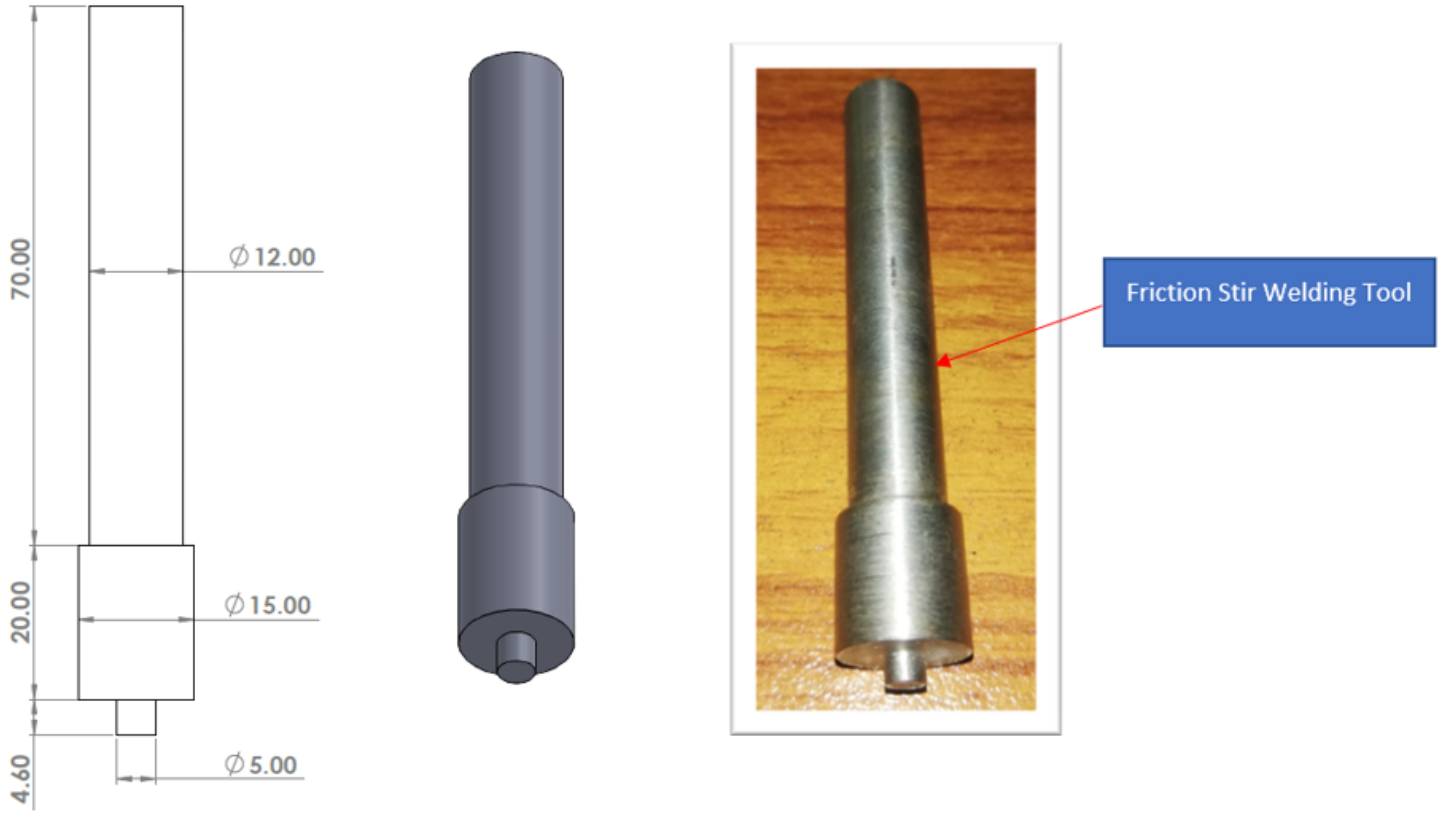


**Figure 5**

FSW Tools Geometry

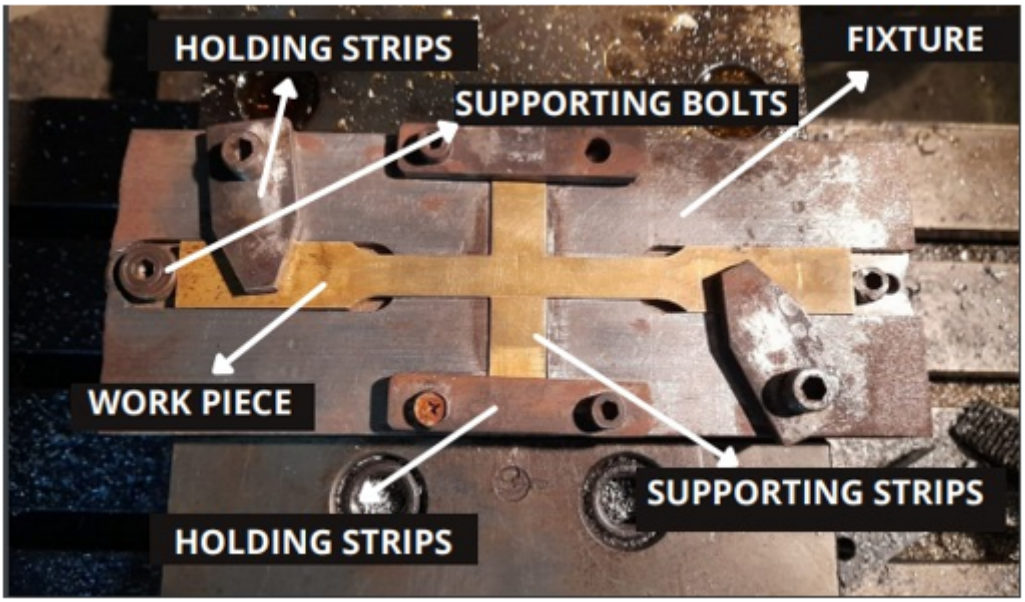


**Figure 6**

Fixture holding the Specimen for FSW

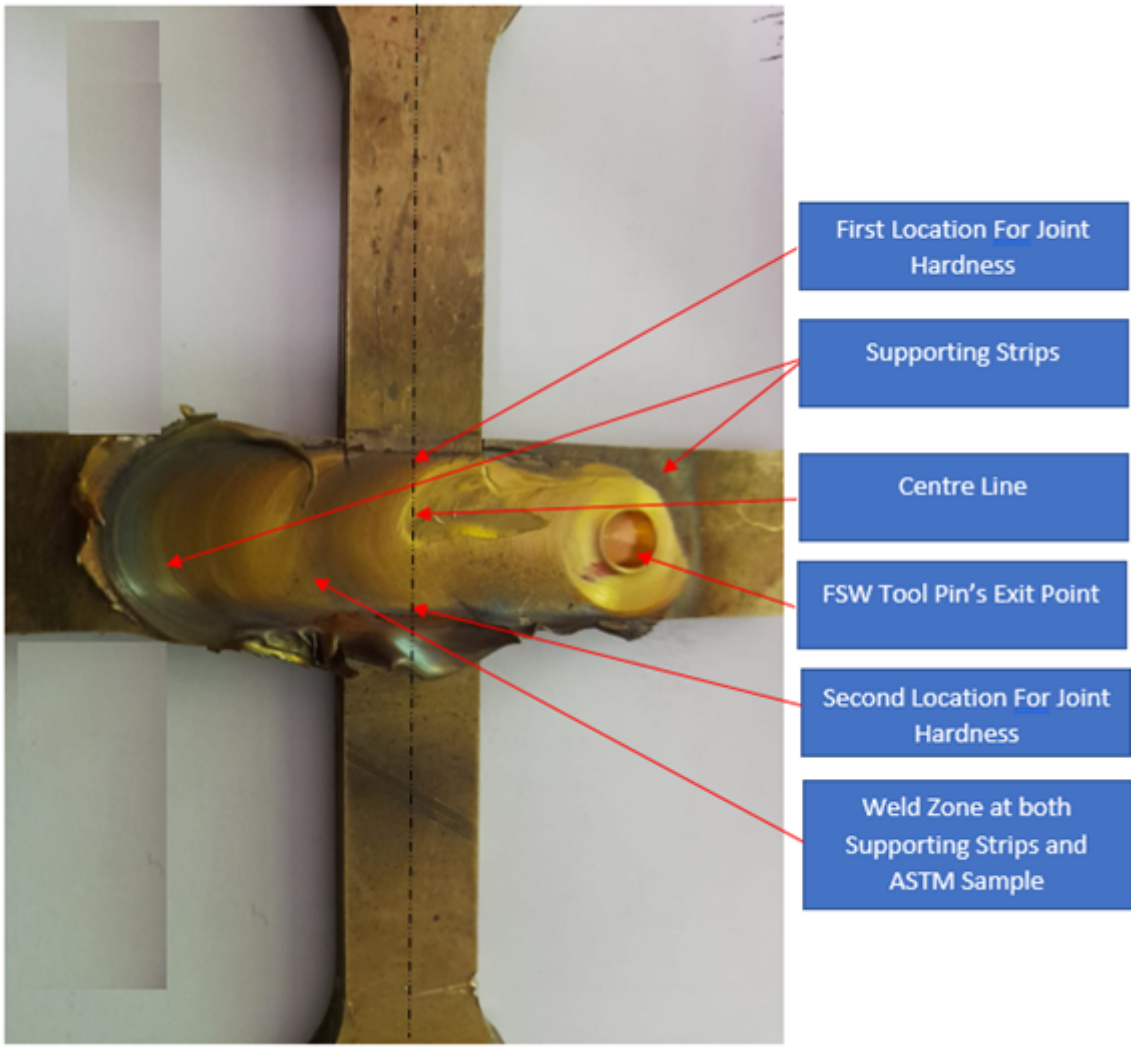


**Figure 7**

A Friction Stir Weld with supporting strips


**Figure 8**

Thermal Imager

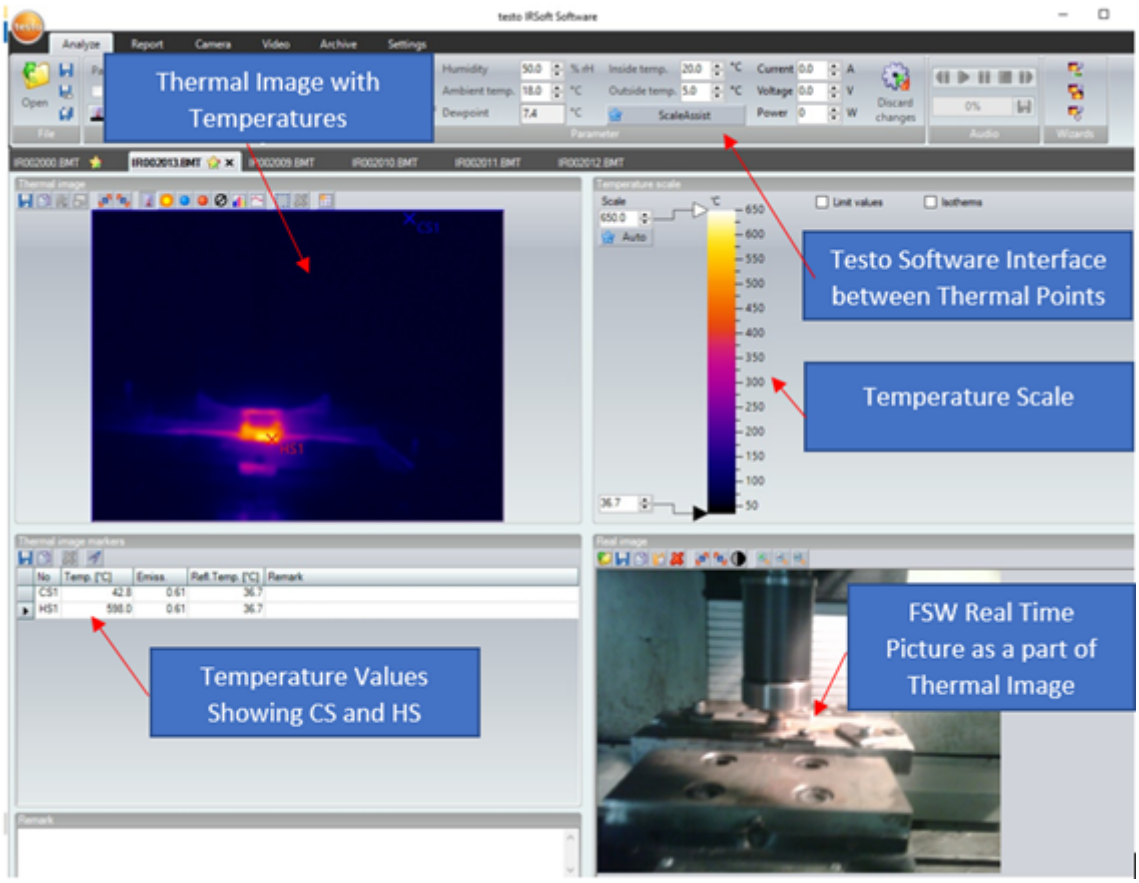


**Figure 9**

An example of Thermal Image from Testo 868 Imager

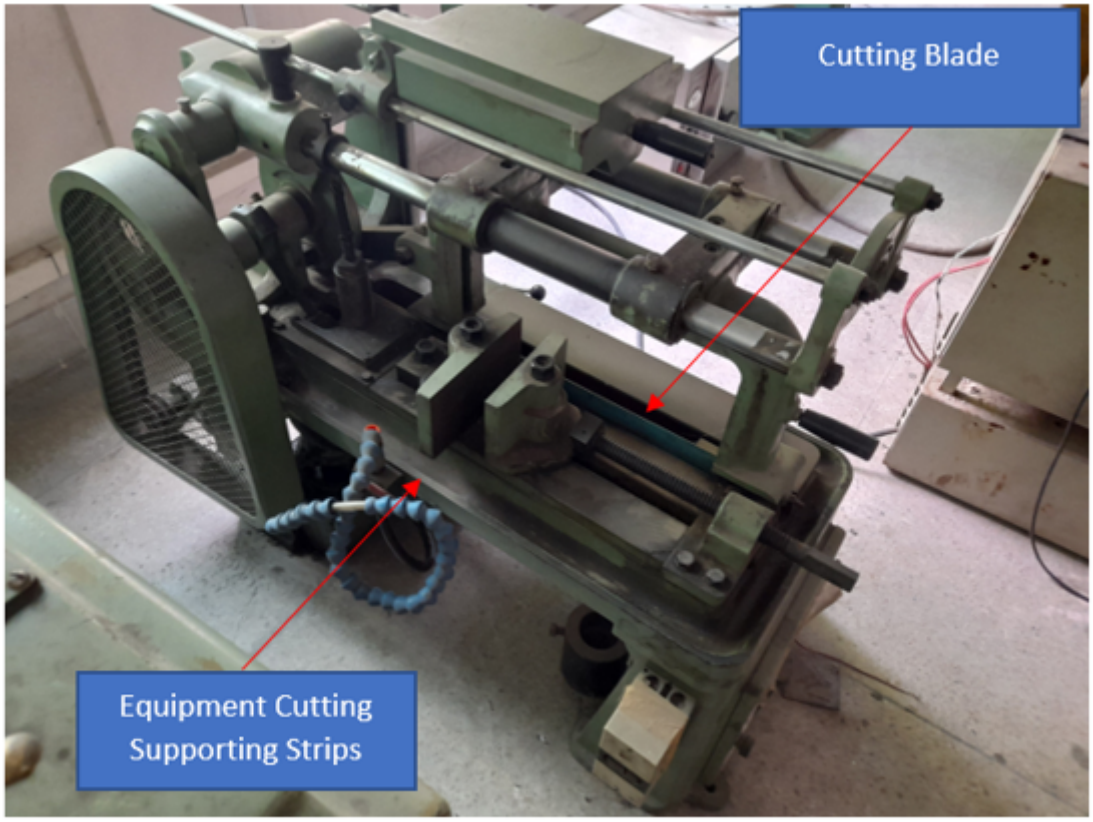


**Figure 10**

Electric Saw Equipment for cutting supporting sides of welded specimens

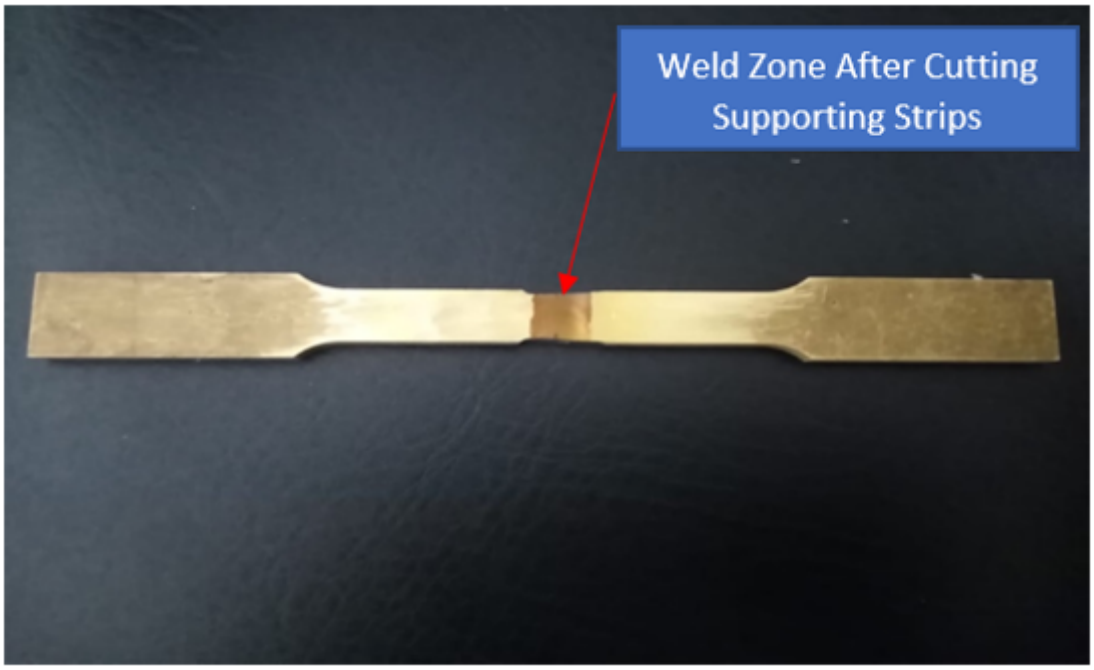


**Figure 11**

A sample Cut by Electric Saw Equipment

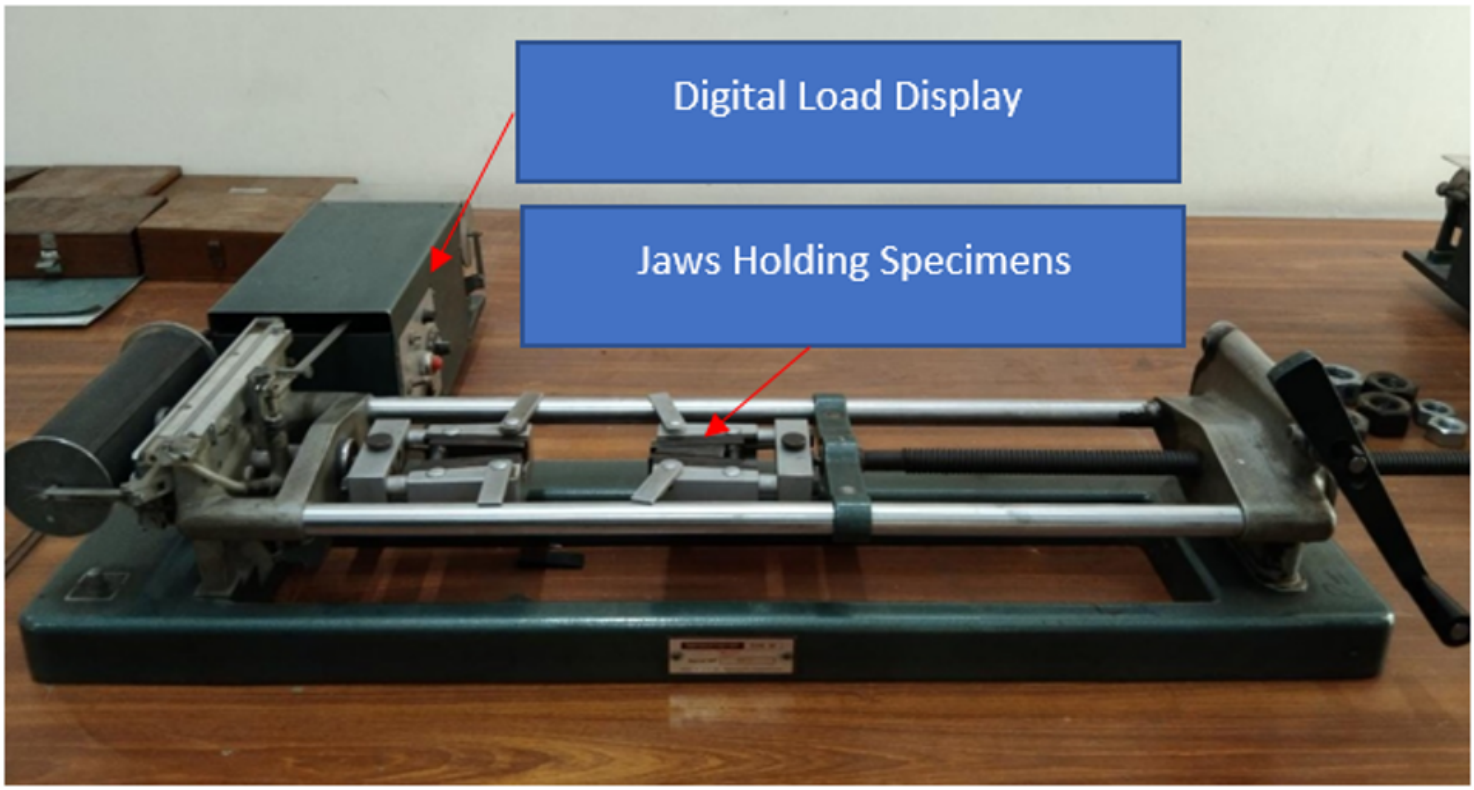


**Figure 12**

Hounsfield Tensometer for measuring Friction Stir Weld Strength (FSWS)


**Figure 13**

A broken FSW Sample

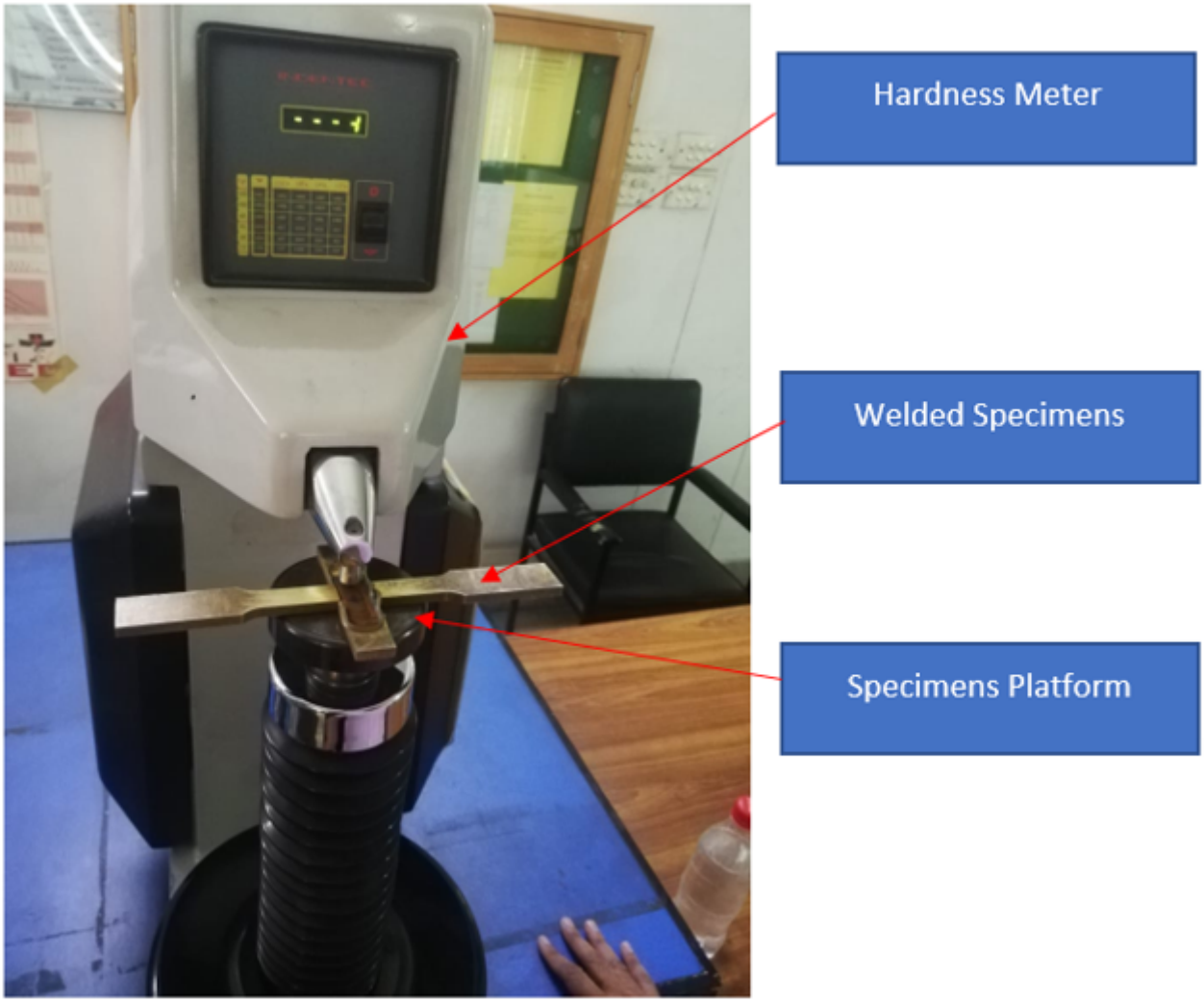


**Figure 14**

Rockwell Hardness Tester

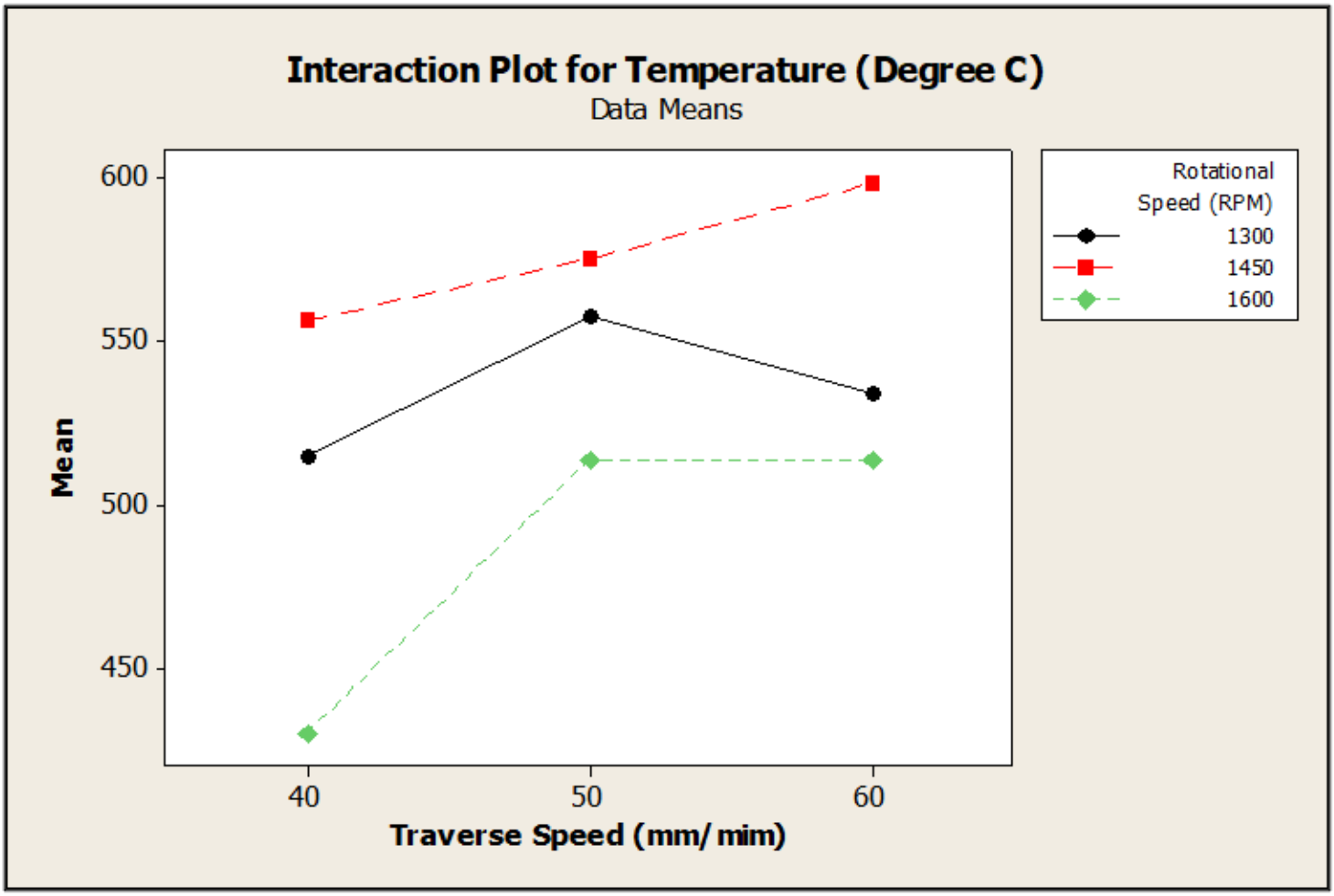


**Figure 15**

Interaction plots between FSWF for weld temperature

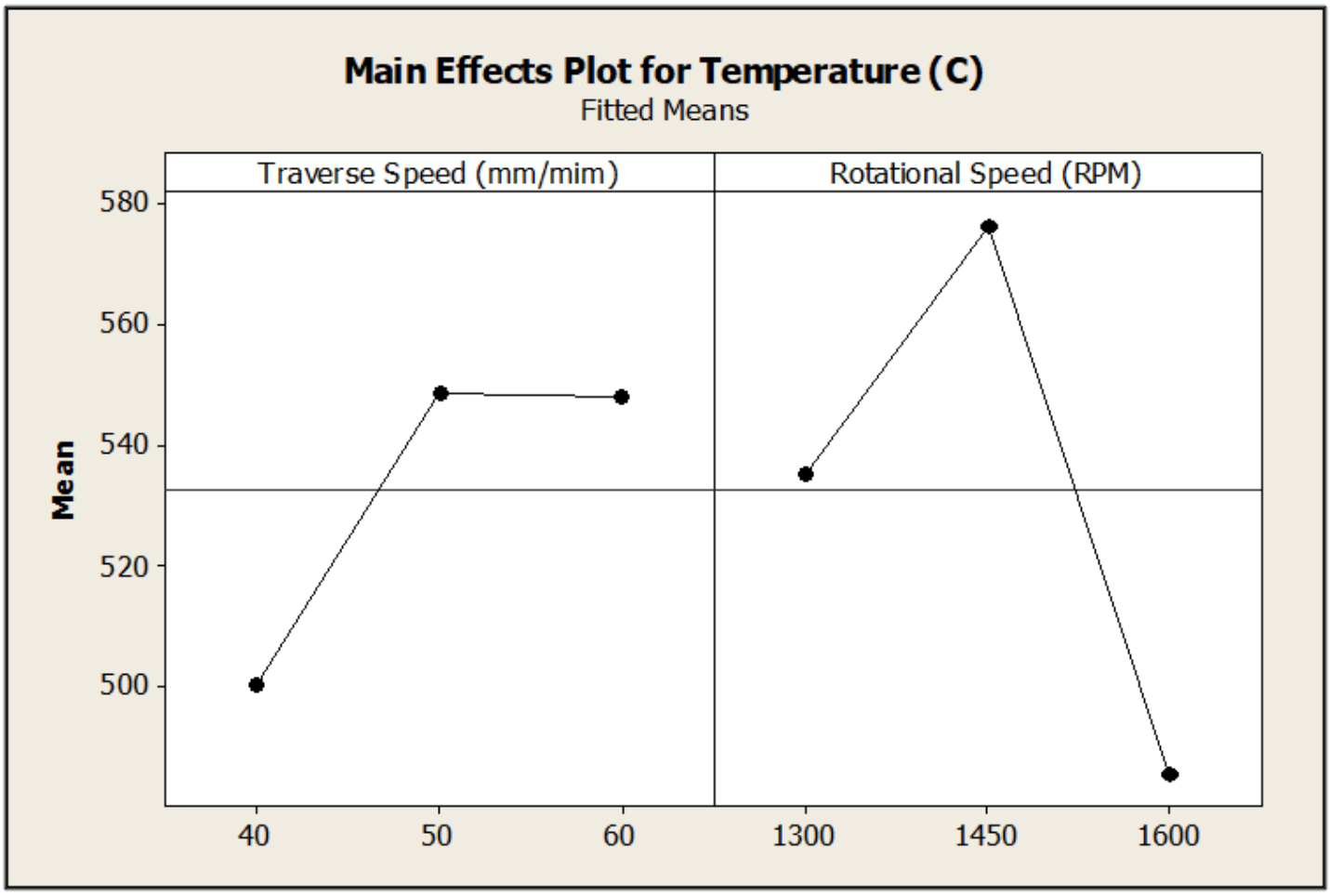


**Figure 16**

Main effects plot for weld temperature

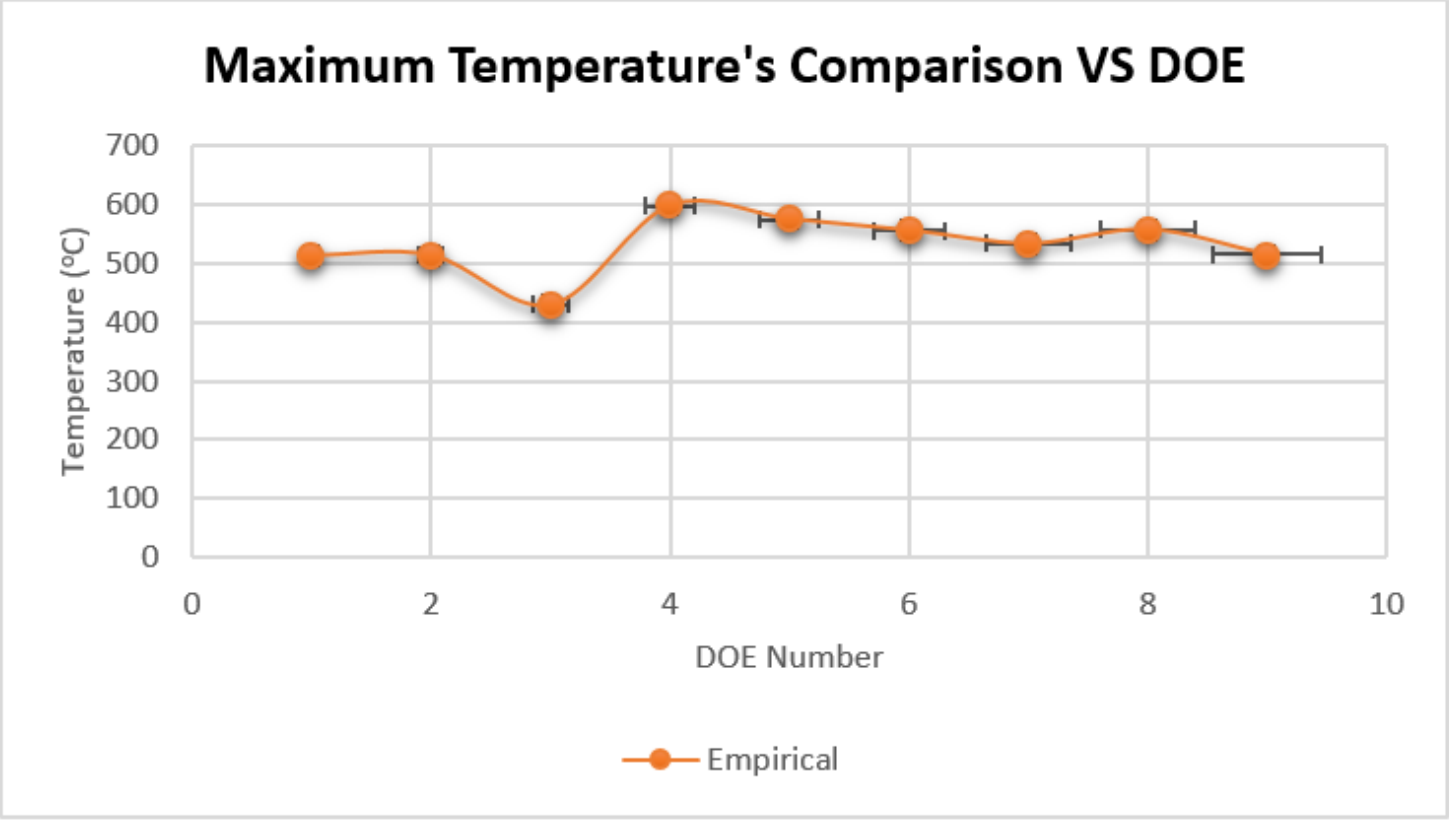


**Figure 17**

Empirical weld temperature for each DOE

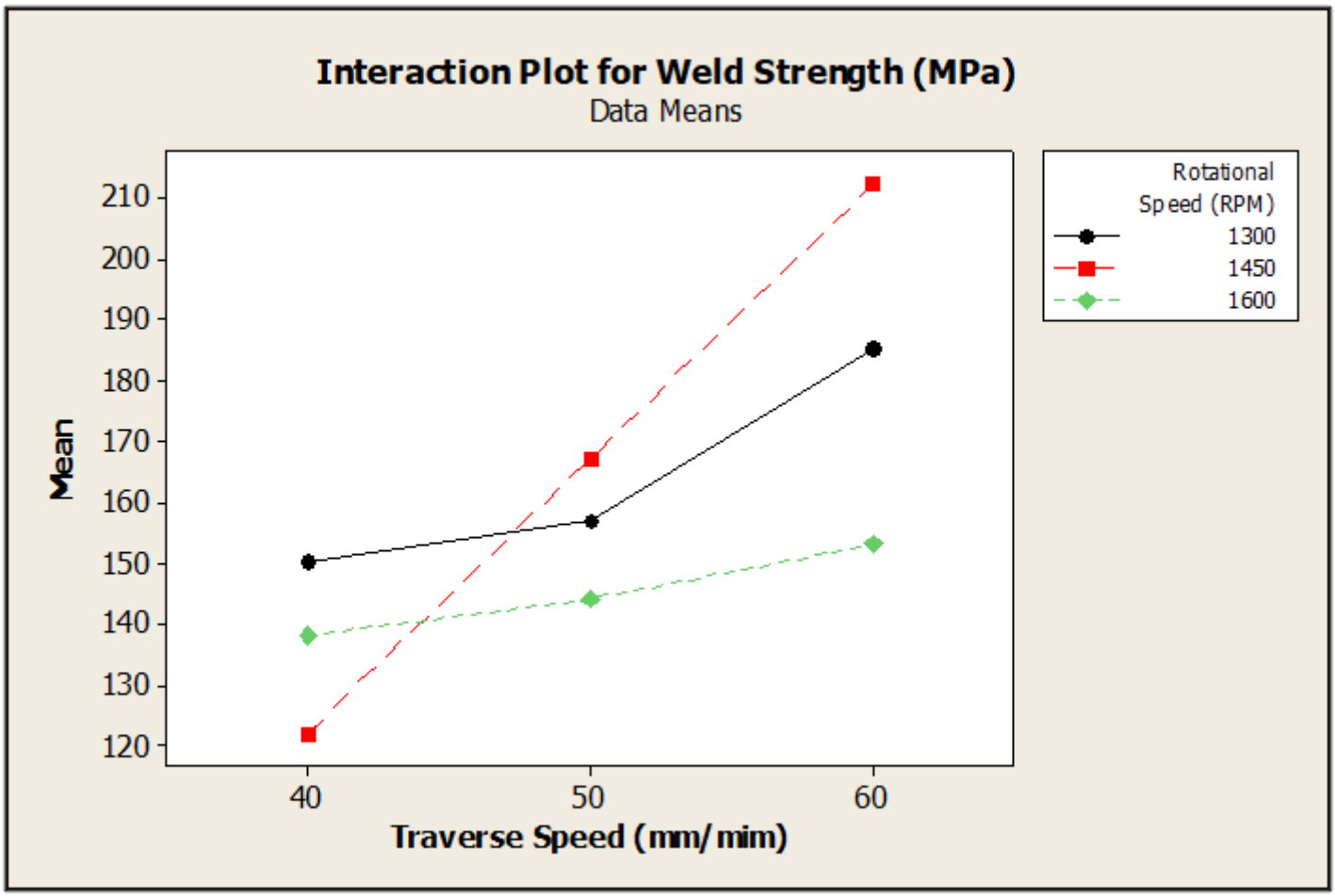


**Figure 18**

Interaction plots between FSWF for weld strength

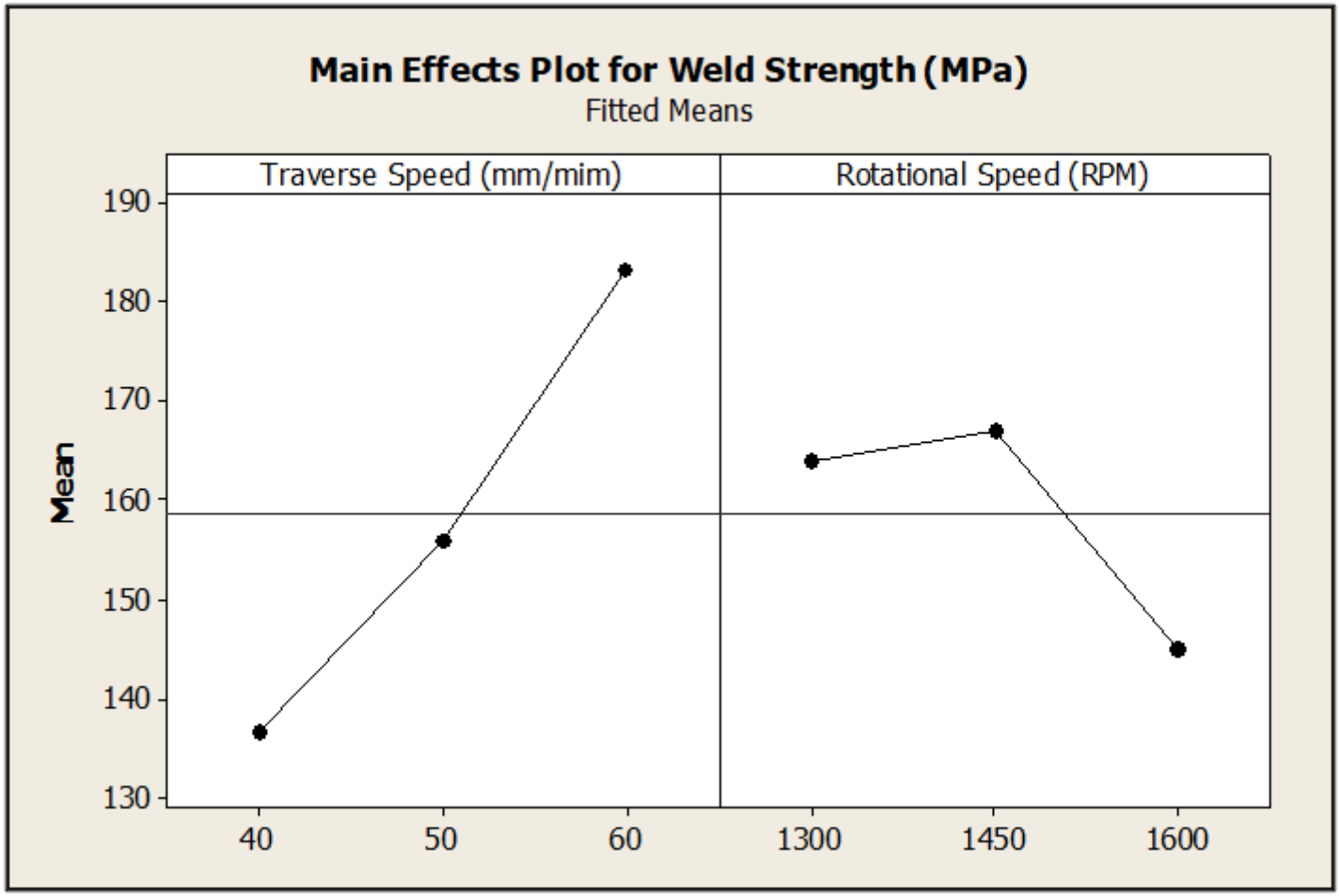


**Figure 19**

Main effects plot for weld strength

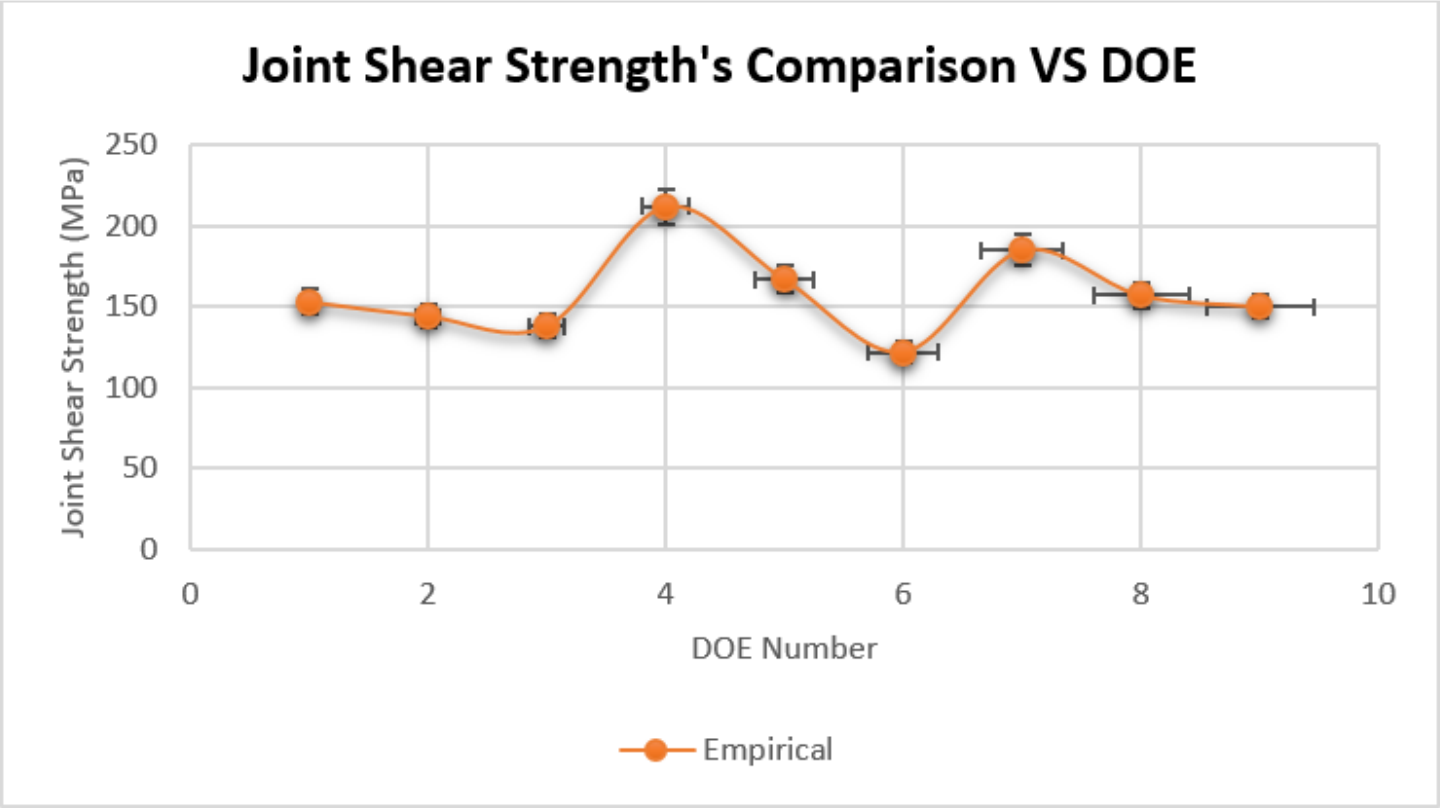


**Figure 20**

Empirical weld strength for each DOE

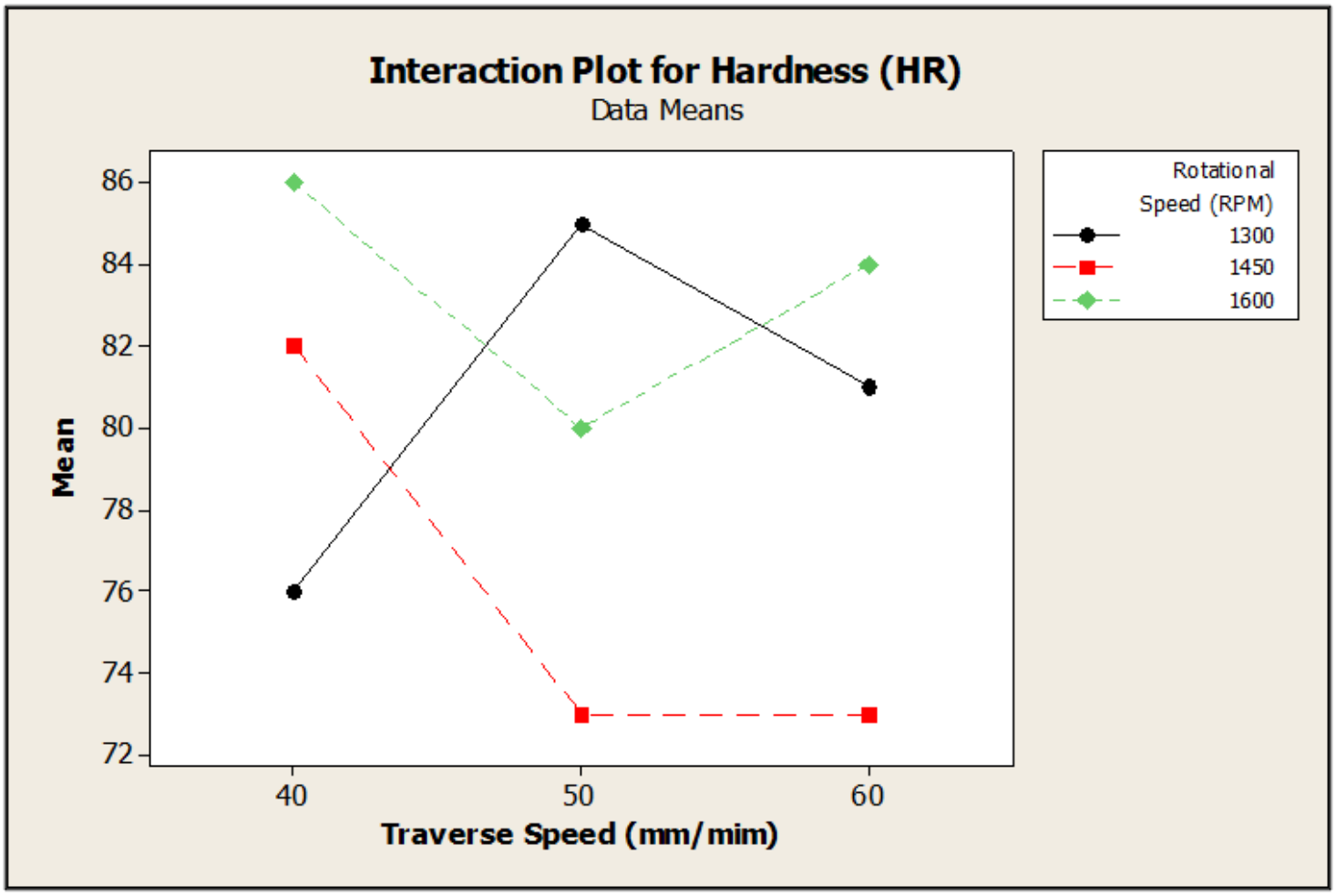


Figure 21

Interaction plots between FSWF for weld hardness

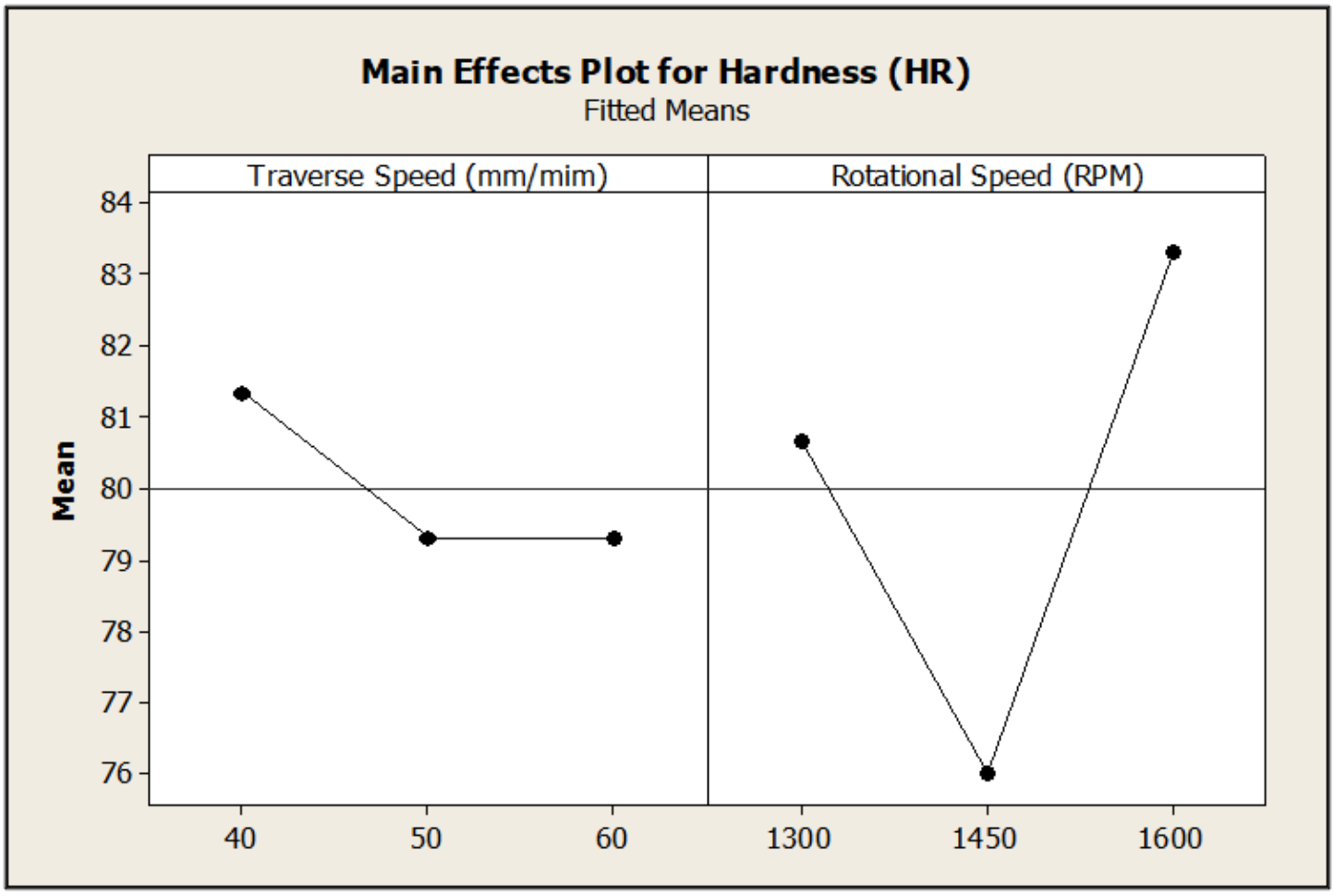


**Figure 22**

Main effects plot for weld hardness

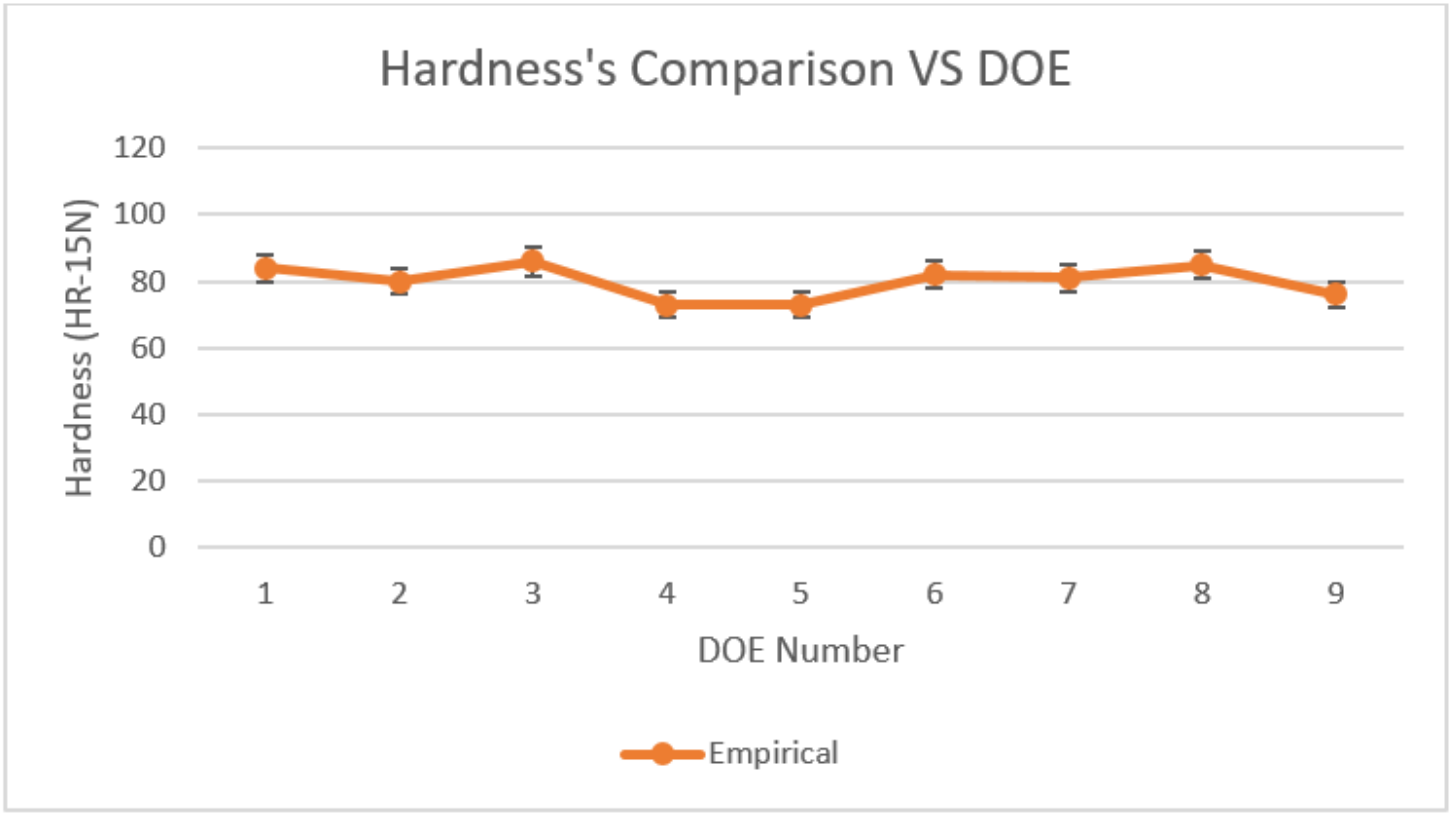


**Figure 23**

Experimental weld hardness for each DOE

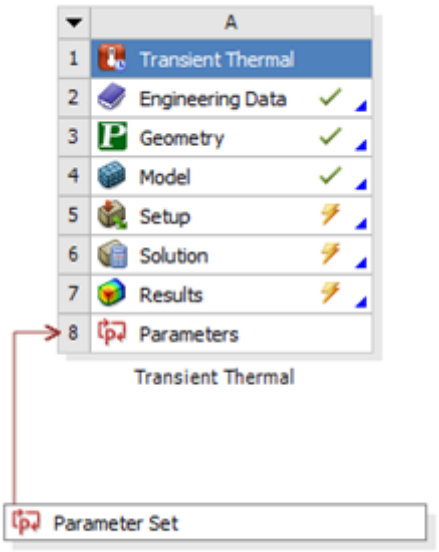


**Figure 24**

Thermal Transient Analysis FEA_A

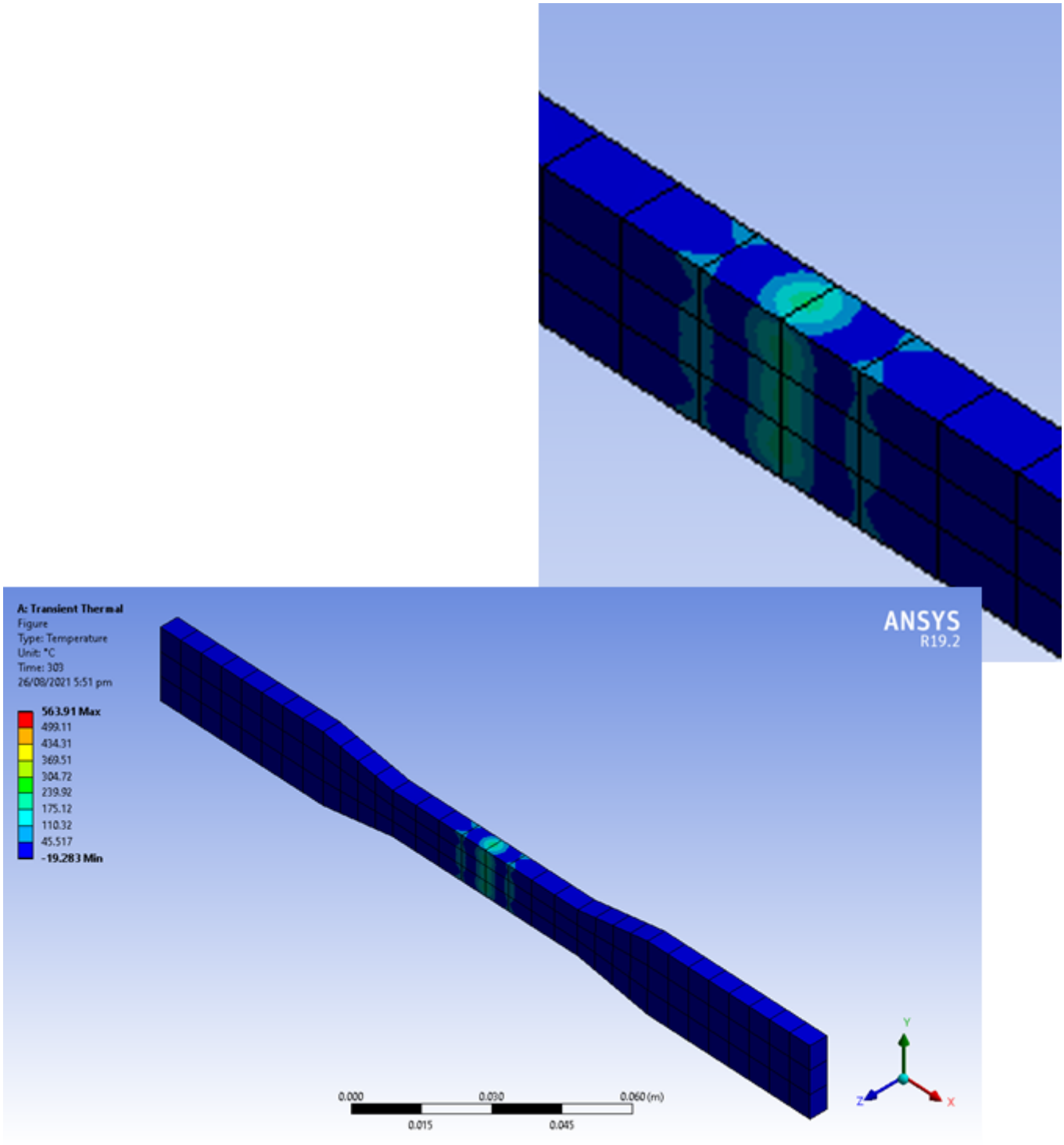


## Figure 25

Numerical results showing maximum and minimum temperatures for DOE 4 with zoomed heated FSWZ

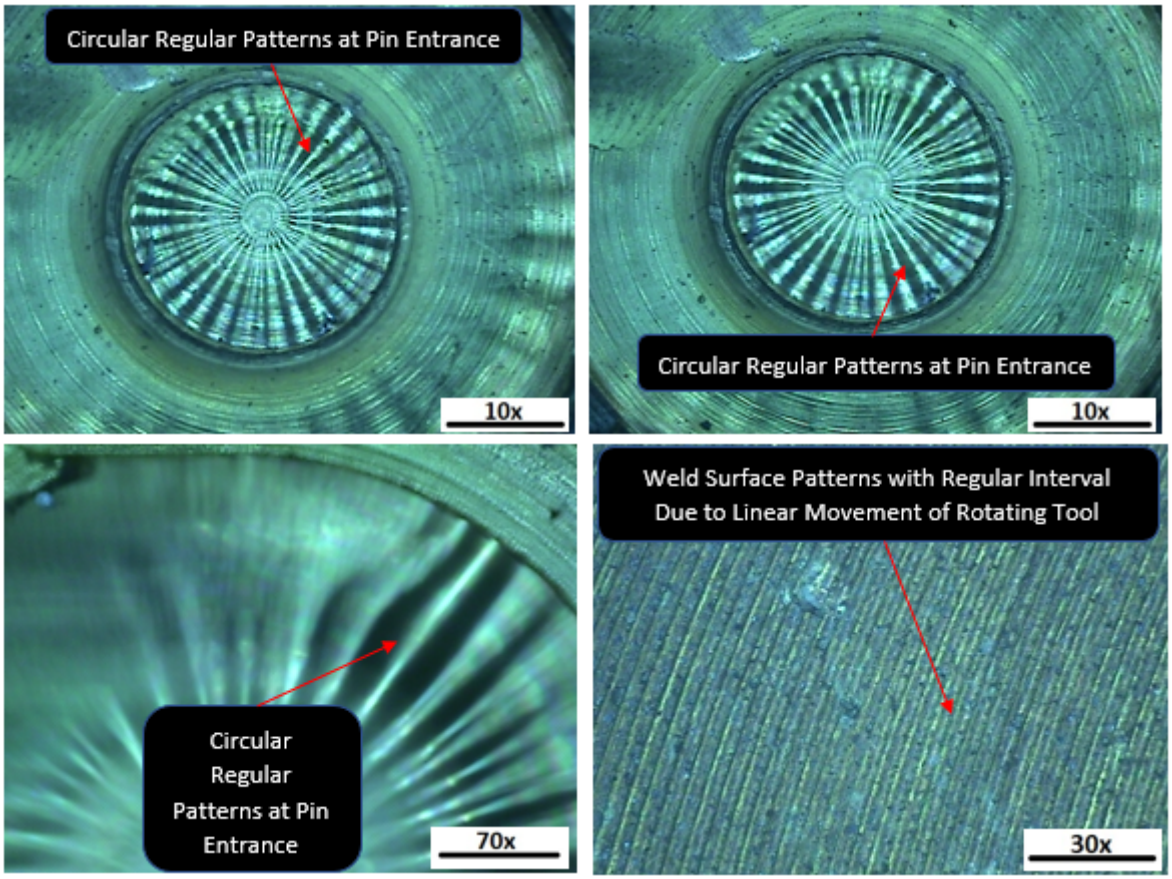


**Figure 26**

Common Circular Pattern

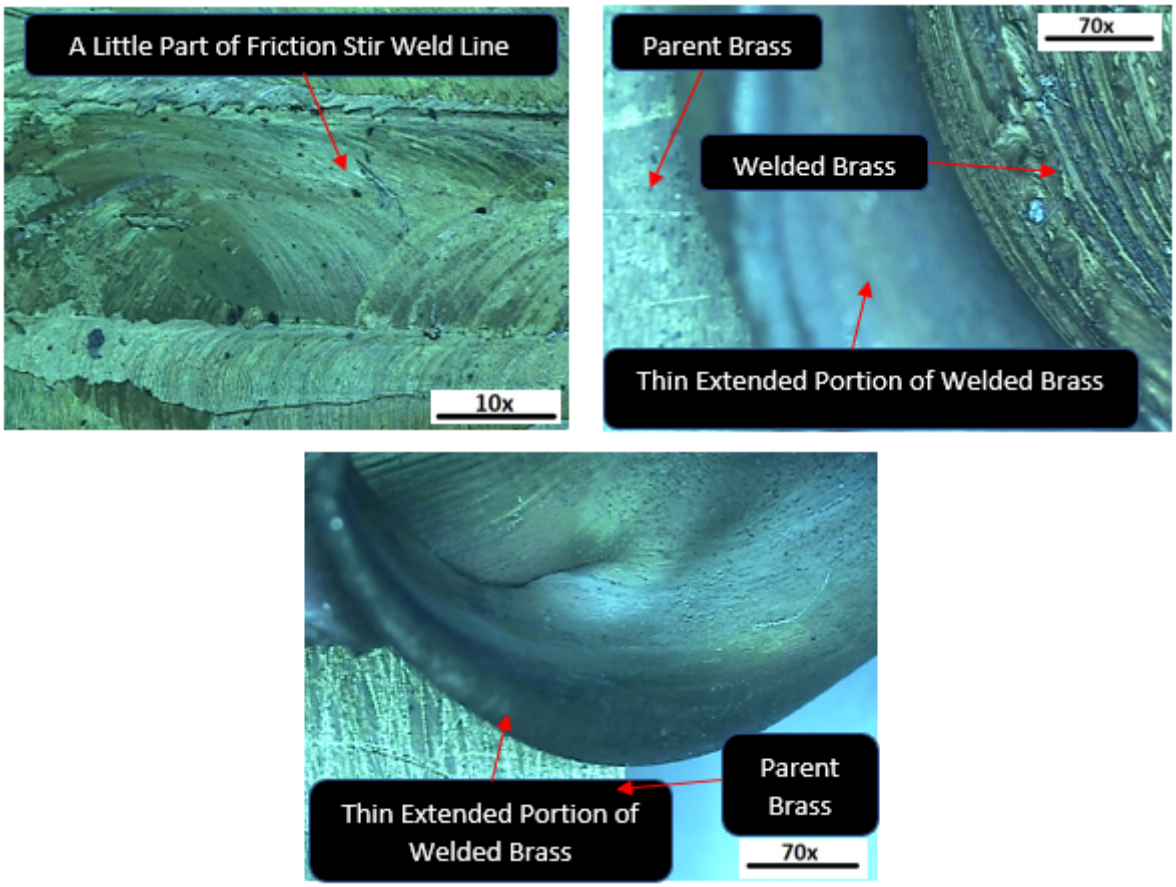


Figure 27

Weld line and extended thin brass after welding

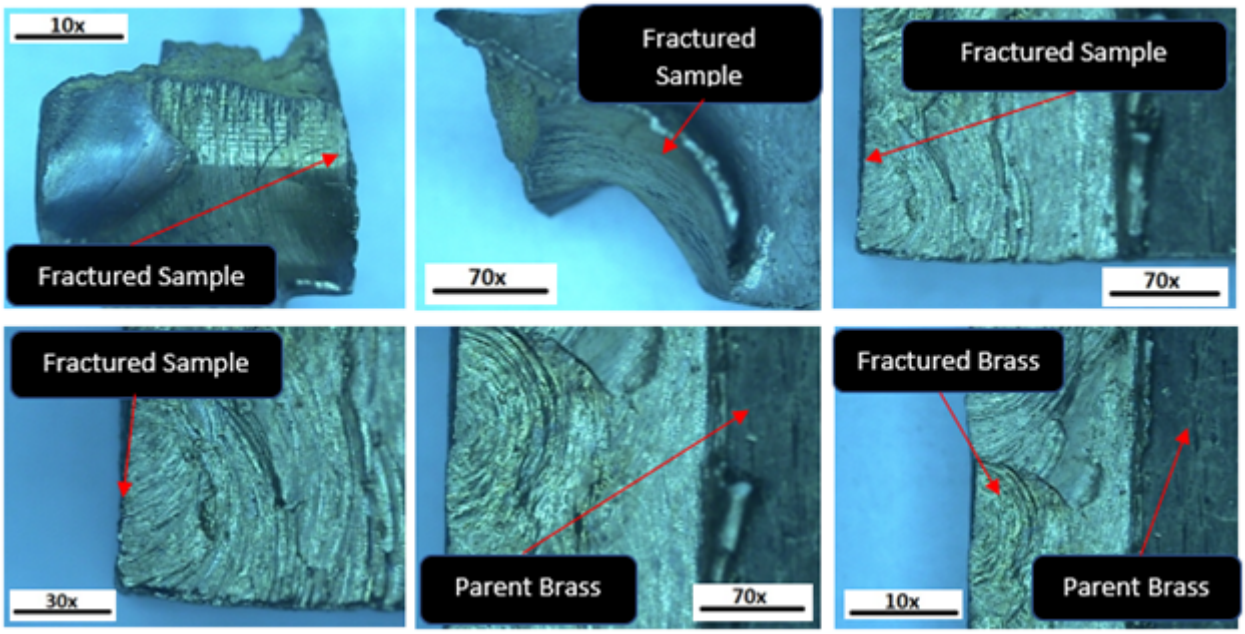


Figure 28

Fractured surfaces and edges

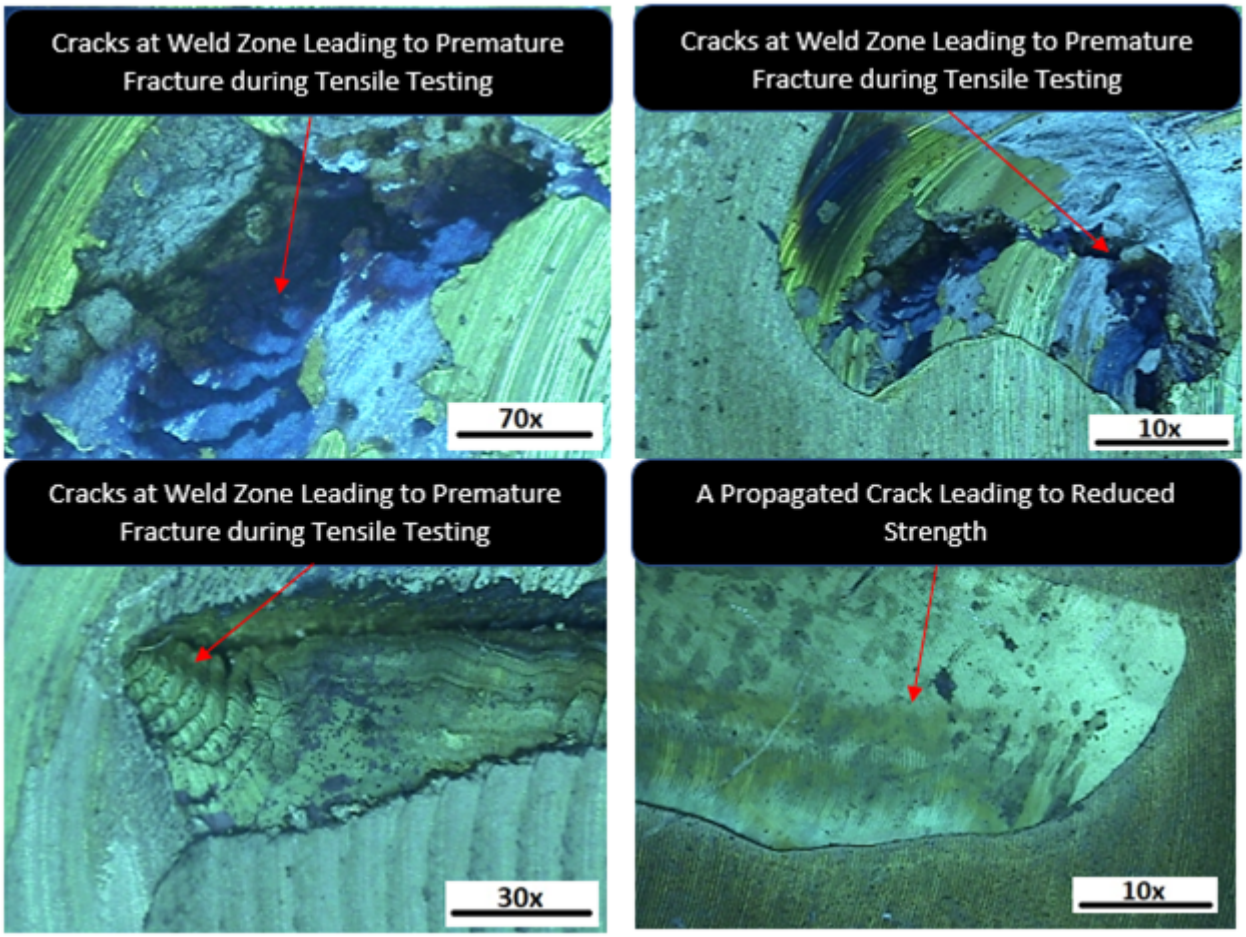


**Figure 29**

Cracks within the welded brass specimens